# Mercury records covering the past 90 kyr from lakes Prespa and Ohrid, SE Europe

Alice R. Paine[1*], Isabel M. Fendley[1], Joost Frieling[1], Tamsin A. Mather[1], Jack H. Lacey[2], Bernd Wagner[3], Stuart A. Robinson[1], David M. Pyle[1], Alexander Francke[4], Theodore R Them II[5], Konstantinos Panagiotopoulos[3]

[1]Department of Earth Sciences, University of Oxford, Oxford, UK, OX1 3AN
[2]National Environmental Isotope Facility, British Geological Survey, Nottingham, UK
[3]Institute of Geology and Mineralogy, University of Cologne, Cologne, Germany
[4] ~~Department~~ Discipline of Archaeology, College of Humanities, Arts and Social Sciences, Flinders University, Adelaide, 5001, Australia
[5]Department of Geology and Environmental Geosciences, College of Charleston, Charleston, SC 29424, USA
*Corresponding Author: alice.paine@earth.ox.ac.uk

## ABSTRACT

The element mercury (Hg) is a key pollutant, and much insight has been gained by studying the present-day Hg cycle. However, many important processes within this cycle operate on timescales responsive to centennial to millennial-scale environmental variability, highlighting the importance of also investigating the longer-term Hg records in sedimentary archives. To this end, we here explore the timing, magnitude, and expression of Hg signals retained in sediments over the past ~90 ka from two lakes, linked by a subterranean karst system: Lake Prespa (Greece/North Macedonia/Albania) and Lake Ohrid (North Macedonia/Albania). Results suggest that Hg fluctuations are largely independent of variability in common host phases in each lake, and the recorded sedimentary Hg signals show distinct differences first during the late Pleistocene (Marine Isotope Stages 2 – 5 ~~5~~). The Hg signals in Lake Prespa sediments highlights an abrupt, short-lived, peak in Hg accumulation coinciding with local deglaciation. In contrast, Lake Ohrid shows a broader interval with enhanced Hg accumulation, and, superimposed, a series of low-amplitude oscillations in Hg concentration peaking during the Last Glacial Maximum, that may result from elevated clastic inputs. Divergent Hg signals are also recorded during the early and middle Holocene (Marine Isotope Stage 1). Here, Lake Prespa sediments show a series of large Hg peaks; while Lake Ohrid sediments show a progression to lower Hg values. Around 3 ka, anthropogenic influences overwhelm local fluxes in both lakes. The lack of coherence in Hg accumulation between the two lakes suggests that, in the absence of an exceptional perturbation, local differences in sediment composition, lake structure, and water balance all influence the local Hg cycle, and determine the extent to which Hg signals reflect local or global-scale environmental changes.

## 1. Introduction

Mercury (Hg) is a volatile metal released into ~~the atmosphere by~~environment ~~-~~from both natural and anthropogenic sources, and actively cycled between surface reservoirs (e.g., atmosphere, ocean,

lakes) ~~processes and human activities~~. Emissions of Hg by geological sources/processes are unevenly distributed across the Earth's surface, and are generally concentrated where tectonic, volcanic, and geothermal activities are most intense (Rytuba, 2003; Edwards et al., 2021; Schlüter, 2000). Geological processes have been major drivers of variability in the global Hg cycle throughout Earth's history (Selin, 2009), leading to the use of sedimentary Hg to reconstruct periods of intense volcanism (e.g., large igneous provinces (LIPs)) in Earth's geological past (e.g., Grasby et al., 2019; Percival et al., 2018). ~~However~~In recent times, Hg release associated with industrialisation, the extraction and combustion of fossil fuels, and natural resources (metals) has overwhelmed the natural background flux (Outridge et al., 2018; Streets et al., 2019; United Nations Environment Programme, 2018).

Existing in the atmosphere primarily in the form of gaseous elemental mercury, Hg has an atmospheric lifetime of up to 2 years, facilitating its deposition far from the original source (Lyman et al., 2020). Once removed from the atmosphere, Hg may enter ~~the terrestrial environment~~vegetation and soils where it is cycled between reservoirs by a complex series of processes, many of which occur on timescales that exceed present-day monitoring (**Fig. 1**) (Branfireun et al., 2020; Selin, 2009). Evasion back to the atmosphere, consumption by living organisms, or sequestration within aquatic sediments all represent ways in which Hg may 'leave' the terrestrial environment, and aquatic sediments are known to be ~~Aquatic sediments are~~ particularly effective sinks within the global Hg cycle (Bishop et al., 2020; Selin, 2009). Here, ~~organic~~ microbial processes lead to the formation of methylmercury (MeHg), which is the most bio-accumulative Hg species and can cause severe neurological and physiological damage to complex organisms if ingested (Driscoll et al., 2013; Wang et al., 2019).

The ecological and societal risks of environmental Hg contamination underscore the importance of quantifying how natural and anthropogenic processes may influence Hg sequestration within aquatic systems, and the timescales upon which they are effective. Time-resolved sediment records sourced from marine and lacustrine basins are highly suitable for assessing these roles further back in time, as the Hg deposited may originate from one of several potential sources in the atmospheric (e.g., precipitation, dust), terrestrial (e.g., soils, detrital matter), aquatic, and/or lithospheric domain (**Fig. 1**). ~~as~~ Thus, they can provide time-resolved records of Hg deposition, cycling, burial, and accumulation relative to changing environmental conditions on a local, regional, or even global-scale (Cooke et al., 2020; Zaferani and Biester, 2021). Therefore, they can offer new insights into the cycling of Hg in the terrestrial realm.

Analysis of pre-industrial marine and ~~lake~~ lacustrine sediment records suggest that Hg ~~composition~~ concentration broadly reflects variability in climate (Li et al., 2020). On orbital (>$10^3$-year) timescales, oceanic Hg signals manifest as low-amplitude fluctuations corresponding to global-scale climate shifts from warm (interglacial) to colder (glacial) conditions; for example due to changes in atmospheric composition (e.g., mineral dust loading) and circulation, biogeochemical cycling (Figueiredo et al., 2022), and/or ocean circulation (Figueiredo et al., 2020; Gelety et al., 2007; Jitaru et al., 2009; Kita et al., 2016). On centennial to millennial ($10^2$-$10^3$-years) timescales, lacustrine Hg signals correspond

more closely to transient changes in hydrology, landscape dynamics, and ice/permafrost extent on local/regional scales (Chede et al., 2022; Cordeiro et al., 2011; de Lacerda et al., 2017; Fadina et al., 2019; Li et al., 2023; Pérez-Rodríguez et al., 2018, 2015) (**Fig. 1**). Importantly, climate-associated Hg signals retained in lacustrine records integrate a range of processes and some records show higher sedimentary Hg concentrations during cold, arid conditions (e.g., Li et al., 2020), while other records tend to have higher Hg concentrations with warm and wet climates. For example, increases in catchment-sourced detrital input have been proposed as the primary cause of Hg enrichment in temperate lakes (Pan et al., 2020; Schütze et al., 2018), and near-shore marine records (Fadina et al., 2019). Conversely, lakes located in glaciated regions may show dilution of Hg by the same inputs (Schneider et al., 2020). Local, site-specific factors are therefore likely to influence sedimentary Hg records. Yet, the combined effects of global and local processes complicate study of how changes in the terrestrial Hg cycle may translate to measurable sedimentary signals and signals that are comparable between different regional or global archives.

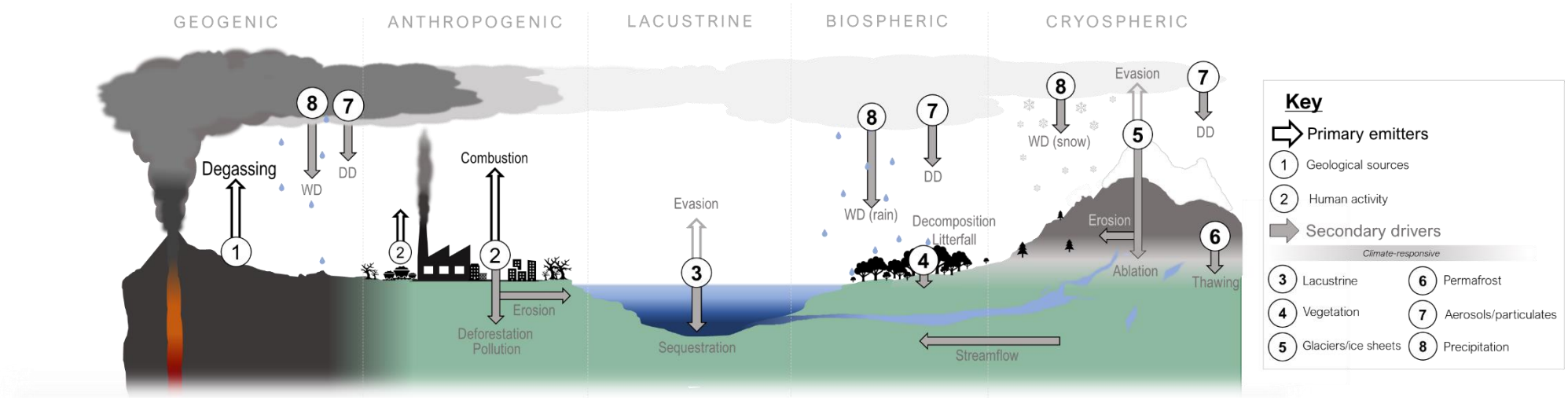


**Figure 1**: A summary diagram depicting the key anthropogenic, geogenic, biospheric, cryospheric, and lacustrine processes, which could generate and modify a sedimentary Hg signal over $10^1$-$10^5$-year timescales. Processes are abbreviated as: WD – wet deposition, DD – dry deposition. Non-filled arrows depict processes acting to increase the atmospheric Hg burden, and colour filled arrows depict processes acting to influence the quantity of Hg stored in terrestrial reservoirs. This figure is schematic (not drawn to scale), and constructed on the basis of reviews by Bishop et al. (2020), Obrist et al. (2018), Selin et al. (2009).

## ~~1.1 Sedimentary mercury records~~

Sedimentary Hg presence (or absence) ~~Sedimentary Hg concentrations~~ at discrete intervals can be quantified using the total Hg concentration ($Hg_T$) (Bishop et al., 2020; Kohler et al., 2022; Nasr et al., 2011). However, internal changes in bioproductivity, organic matter type and/or flux, sedimentation rate, pH, and redox conditions could all produce a distinct, local, transient, sedimentary Hg enrichment without a meaningful change in the total amount of Hg present and/or mobile in the broader aquatic system. In light of these complexities, it has become common practice to examine total Hg concentration ($Hg_T$) alongside Hg concentration divided by (normalised to) the concentration of various chemical species~~normalized Hg~~. Normalisation is often applied when it can be shown that the abundance of a carrier (or "host") phase directly impacts Hg content. Normalisation (e.g. Hg/total organic carbon (TOC), Hg/total sulphur (TS)) may, in those cases, then reveal broader changes in environmental Hg availability ~~This impact is then removed, via normalisation (e.g. Hg/TOC, Hg/TS), to reveal changes in environmental Hg availability~~ (Grasby et al., 2019; Percival et al., 2015; Shen et al., 2020; Them et al., 2019). Such an approach is particularly beneficial for studies typically spanning >$10^2$-year timescales, where the goal is to isolate the effects of local depositional and/or transport processes on Hg signals recorded in the sediment through time.

Organic matter (hereafter represented by total organic carbon (TOC)) is generally considered the dominant carrier phase of sedimentary Hg (Chakraborty et al., 2015; Ravichandran, 2004). For records in which TOC and Hg co-vary linearly, Hg is generally normalized to TOC (Chede et al., 2022; Figueiredo et al., 2022~~a~~, 2020; Kita et al., 2016~~a~~; Outridge et al., 2019). Some systems do not exhibit a relation to TOC and Hg may instead be adsorbed onto (fine-grained) detrital minerals and detected by a correlation between Hg and mineral~~-~~dominating elements such as aluminium (Al), titanium (Ti), zirconium (Zr), rubidium (Rb), or potassium (K) (Sanei et al., 2012; Sial et al., 2013; Them et al., 2019). In few cases, sulphide minerals may act as important Hg hosts (Benoit et al., 1999; Han et al., 2008), however this is less common in freshwater lacustrine systems where sulphate-reduction is often limited and only a small fraction of non-organic sulfur is buried (Ding et al., 2016; Holmer and Storkholm, 2001; Tisserand et al., 2022; Watanabe et al., 2004).

Mercury's relationship with other sedimentary components is often complex. For example, $Hg_T$ may also be suppressed through dilution by Hg-poor detrital or biogenic (carbonate, silica) material, and Hg in many sediments is not exclusively or clearly modulated by balances between host-phase abundance and dilution. Notably, this can also occur when the host-phases are always present in sufficient quantities to sequester available Hg. In such cases, and where (single) host-phase abundance or dilution cannot be easily accounted for, Hg accumulation rate ($Hg_{AR}$) ~~-~~may provide the most optimal assessment of Hg availability through time as long as a robust age model is available for the archive.

Sedimentary TOC, total sulphur (TS), and detrital and biogenic mineral concentrations change in space and time, underscoring the need to assess how Hg covaries in relation to different host phases and other sedimentary materials. Hydrology, sedimentation regime, and geochemistry may each

influence mercury host-phase availability and burial in a lacustrine system, and are likely to change through time, highlighting the importance of investigating the longer-term records of Hg burial and accumulation in sedimentary archives.

This study explores the timing, magnitude, and expression of Hg signals retained in the sediment records of Lake Prespa (Greece/Albania/North Macedonia) and Lake Ohrid (North Macedonia/Albania) over the past ~90 ka. The two lakes are located only ~10 km apart (**Fig. 2**), are hydrologically connected by karst aquifers with ~50% of water inflow to Lake Ohrid originating from Lake Prespa (Matzinger et al., 2006), and their sediments encode records of environmental change in southeast Europe over the last ~90 ka (Damaschke et al., 2013; Francke et al., 2016; Leng et al., 2010; Panagiotopoulos et al., 2014; Sadori et al., 2016; Wagner et al., 2010). Comparison of their sedimentary records provides a rare opportunity to explore three important questions. First, we test how ~~does~~ the local sedimentary environment (e.g., host phase availability and sources) influences Hg burial.~~?~~ Second, ~~do~~ we investigate whether Hg signals reflect changes in catchment hydrology, structure, and/or varying degrees of interaction between the two lake systems.~~?~~ Finally, we explore whether ~~could~~ regional-scale climate variability could have measurably affected the Hg signals retained in the sediments.~~?~~

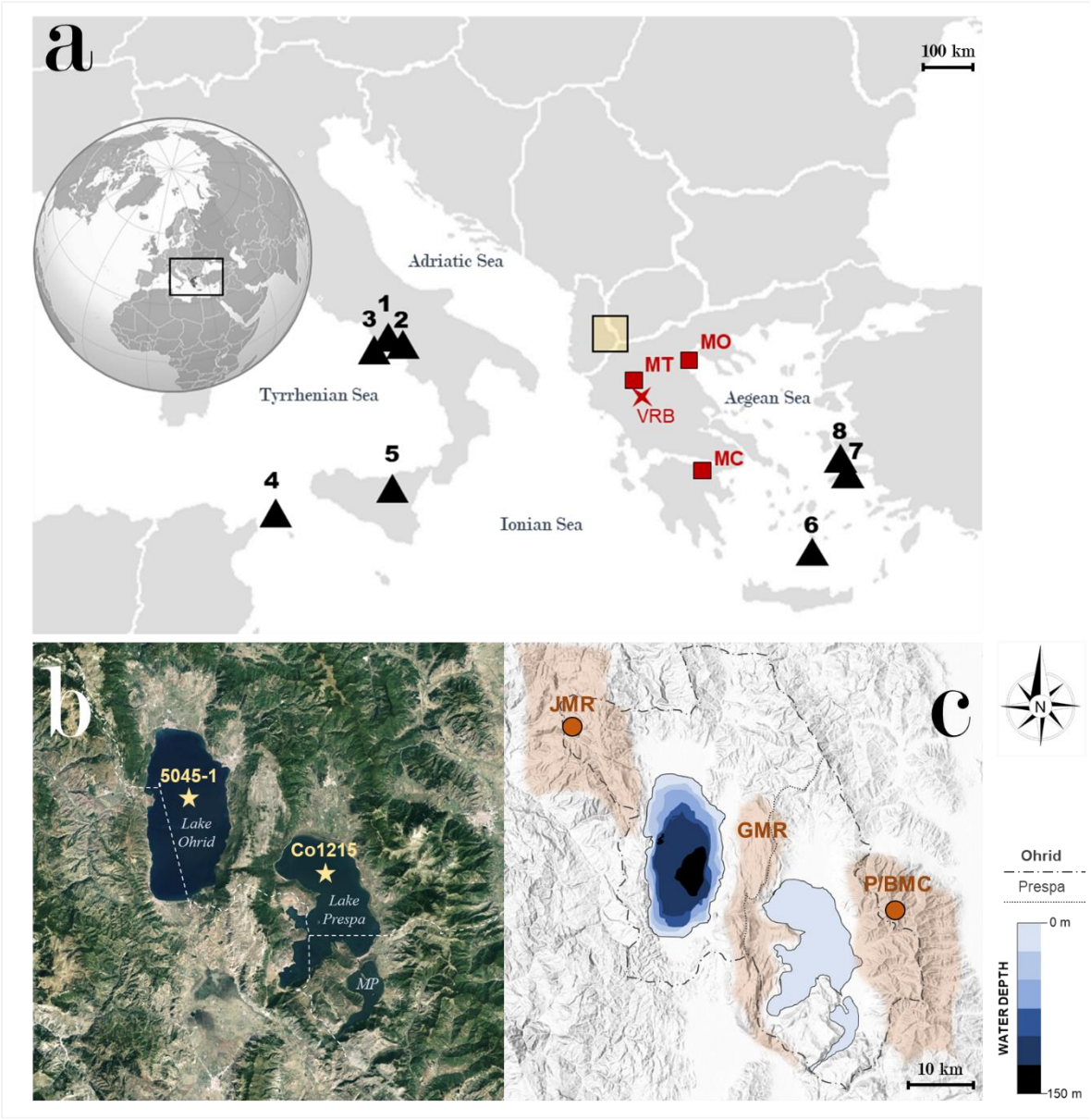


**Figure 2**: (a) Map showing the location of lakes Prespa and Ohrid within Southern Europe (yellow shaded box). Volcanoes from which tephra has been identifed in Co1215 (Prespa) and/or 5045-1 (Ohrid) are coloured as black triangles, and numbered as: 1 – Vesuvius, 2 – Campi Flegrei, 3 – Ischia, 4 - Pantelleria, 5 – Etna. Volcanoes of the South Aegean Volcanic Arc with known explosive eruptions (>magnitude 4.0) between 90 and 0 ka are also numbered: 6 – Santorini, 7 – Nisyros, 8 – Yali. Sites referred to in this study are also labelled as follows: (red squares) MT – Mount Tymphi, MO – Mount Olympus, MC – Mount Chelmos; (red star) VRB – Voidomaitis river basin. (b) Aerial photo showing the coring locations of Co1215 and 5045-1, and illustrating the vegetation distributions of the area surrounding lakes Prespa and Ohrid. Mikri Prespa is labelled as 'MP'. Base image sourced from GoogleEarth v 9.177.0.1™. (c) Hillshade map of the Prespa/Ohrid region and bathymetric data of lakes Prespa and Ohrid (Jovanovska et al., 2016; Wagner et al., 2022). Grey dashed lines denote watershed boundaries for lakes Prespa and Ohrid , respectively adapted from Panagiotopoulos et al. (2019). Basemap sourced from ArcGIS v 10.0™ (spatial reference 102100 (3857)). Orange shading denotes mountain ranges are labelled as: P/BMC – Pelister/Baba mountain chain (circle marking the location of Mount Pelister: 2601 m a.s.l), GMR – Galičica mountain range, and JMR – Jablanica mountain range (circle marking the location of Jablanica Mountain - 2257 m a.s.l). All mountain ranges contain evidence for the presence of glaciers and/or (peri)glacial features of late Pleistocene age (Hughes et al., 2022, 2023)

144

# 2. Site Description

## 2.1. Regional Climate

The Mediterranean Sea and the European continent are both major influences on present-day climate of the region surrounding lakes Prespa and Ohrid. Summer months (July to August) are hot and dry (average monthly air temperature +26 °C) while winter months (November to January) are cold, cloudy and wet, with an average monthly air temperature of −1 °C (Matzinger et al., 2006). Annual precipitation in the region averages ~750 mm $yr^{-1}$, with winter precipitation falling predominantly as snow at high elevations (Hollis and Stevenson, 1997).

Major shifts in sedimentation and catchment structure of lakes Prespa and Ohrid generally correspond to the large-scale climate oscillations captured by proxy records across southern Europe throughout the last glacial-interglacial cycle (~100-kyr) (e.g., Rasmussen et al., 2014; Sanchez Goñi and Harrison, 2010; Tzedakis et al., 2006). Generally higher local temperatures and moisture availability are observed during the last interglacial (pre-74 ka), following which conditions became distinctly colder and/or drier. This resulted in the rapid recession of forest ecosystems, intense erosion of local soils and catchments, and elevated aeolian activity (e.g., Panagiotopoulos et al., 2014; Sadori et al., 2016; Francke et al., 2016). Although slightly warmer conditions were restored between ~57 and 29 ka, both moisture availability and temperature dropped again during the Last Glacial Maximum (LGM; ~29 – 12 ka) – favouring the growth and development of glaciers and (peri)glacial features (e.g., moraines) in the Prespa/Ohrid catchment (Ribolini et al., 2018; Gromig et al., 2018; Ruszkiczay-Rüdiger et al., 2020), but also across the Balkan peninsula (Allard et al., 2021; Hughes and Woodward, 2017; Leontaritis et al., 2020). Lake Prespa's sediments host evidence for millennial scale climate varaiblity during the Last Glacial, which were tentatively correlated to Heinrich Events in the North Atlantic (Wagner et al., 2010). At ~12 ka, the Pleistocene to Holocene transition saw the rapid propagation of warmer, wetter conditions across the region (known as Termination I) with only brief excursions from this warming trend, such as episodes of transient drying and/or cooling at 8.2 ka and 4.2 ka (Bini et al., 2019; Aufgebauer et al., 2012a). Anthropogenic influence on the Balkan landscape becomes increasingly clear from ~2.5 ka onwards, mainly in the form of increased erosion regimes, forest clearance, agricultural land modification, and evidence for metallurgic practices (Panagiotopoulos et al., 2013; Cvetkoska et al., 2014; Radivojević and Roberts, 2021).

~~Present-day vegetation in the Prespa/Ohrid region comprises a mixture of Balkan endemic, central European, and Mediterranean species (Donders et al., 2021; Panagiotopoulos et al., 2014, 2020; Sadori et al., 2016). During the last glacial-interglacial cycle (~100-kyr), sedimentary pollen records from lakes Prespa and Ohrid show three primary stages of vegetation distribution at mid/low altitudes in the catchment: (1) forested, (2) open with significant presence of deciduous trees, and (3) open with significant presence of evergreen vegetation (Panagiotopoulos et al., 2014; Sadori et al., 2016). The timing of shifts in vegetation generally corresponds to the large-scale climate oscillations captured by terrestrial and marine proxy records across the Northern Hemisphere (e.g., Rasmussen et al., 2014; Sanchez Goñi and Harrison, 2010; Tzedakis et al., 2006). Warmer and wetter interglacial~~

~~conditions generally correspond to a more forested catchment in the Prespa/Ohrid region, and cooler, drier conditions correspond to a more open catchment.~~

~~The Balkan Peninsula contains evidence for recurrent glaciation during the late Quaternary (Hughes et al., 2022). Radiometric dating of moraines, boulders, and outwash sediments indicate that glaciers present in high-altitude regions reached their peak volume and/or extent between ~40 and 23 ka (Allard et al., 2021; Hughes and Woodward, 2017; Leontaritis et al., 2020). Evidence for moraine formation on Mount Pelister (~10 km NE of Lake Prespa) (Ribolini et al., 2018) and Mount Jablanica (~15 km NW of Lake Ohrid) (Ruszkiczay-Rüdiger et al., 2020) (**Fig. 2**), and identification of glacial tills and moraine deposits in the Presa/Ohrid catchment (Belmecheri et al., 2009; Gromig et al., 2018) provides further evidence that glaciers and (peri)glacial features were present in the catchment during the late Pleistocene.~~

## 2.2. Lake Prespa

The Prespa lake system (40°54' N, 21°02' E) is composed of two lakes separated by an isthmus and located on the tripoint of North Macedonia, Albania and Greece, at an altitude of 844 metres (m) ~~a.s.l~~above sea level. The ~1300 km$^2$ catchment of the Prespa lakes encompasses the Pelister Mountains to the east and the Galiçica Mountains to the southwest and west (**Fig. 2**). Here we focus on Megali Prespa (hereafter referred to as Lake Prespa), the larger of the two lakes, which has a surface area of 254 km$^2$, a maximum water depth of 48 m, and a mean water depth of 14 m. The total inflow into Lake Prespa averages ~16.9 m$^3$ s$^{-1}$ (Matzinger et al., 2006). Water input is sourced from ~~river~~ surface runoff (56%), direct precipitation (35%), and inflow from the smaller of the two lakes (Mikri Prespa; 9%) (Matzinger et al., 2006). Lake Prespa has no surface outflow. The residence time of the lake's waters is ~11 years (Matzinger et al., 2006) and water is predominantly lost through evaporation (52%), underground karst channels into Lake Ohrid located 10 km to the west (46%), and irrigation (2%). The lake is currently mesotrophic with an average total phosphorus (TP) concentration of 31 mg m$^{-3}$ in the water column, basal anoxia in summer months, and generally clear waters; all signalling moderate biological productivity (Hollis and Stevenson, 1997). However, the lake likely held a more oligotrophic (low) nutrient status during the colder late Pleistocene, where biological producity reduced substantially (Matzinger et al., 2006; Wagner et al., 2010).

## 2.3. Lake Ohrid

Lake Ohrid (41°02′ N, 20°43′ E) lies 693 m ~~a.s.~~above sea level~~l~~. Separated from Lake Prespa by the Galiçica Mountains, the lake straddles the boundary between North Macedonia and Albania (**Fig. 2**). The lake is ~30 km long and 15 km wide, with a maximum water depth of 293 m, water volume of 55.4 km$^3$, and hydraulic residence time of ~70 years. Water input is sourced from direct precipitation (23%), river inflow (24%), and karst springs (53%) fed by precipitation and water from Lake Prespa (Matzinger et al., 2006; Lacey and Jones, 2018), and this hydrological link increases the Ohrid

catchment by ~1300 km$^2$ to ~2610 km$^2$. Evaporation (40%) and outflow via the river Crn Drim (60%) are the dominant pathways for water loss from Lake Ohrid, and complete mixing of the lake occurs only every few years (Matzinger et al., 2006). The present-day lake shows low levels of biological productivity (oligotrophic) with an average dissolved phosphorus content of 4.5 mg m$^{-3}$, and regular mixing maintains moderately oxygenated bottom waters (Matzinger et al., 2006; Wagner et al., 2010).

# 3. Methods

## 3.1. Lake Prespa (Co1215)

Composite core Co1215 was recovered in autumn 2009 and summer 2011 from the central-northern section of Lake Prespa (40°57'50" N, 20°58'41" E, **Fig. 2**). Sediment recovery was performed using a floating platform, with a gravity corer for surface sediments and a 3-m-long percussion piston corer (UWITEC Co. Austria) for deeper sediments. Overlapping 3-m-long sediment cores were cut into segments of up to 1 m in length for transport and storage. After splicing and correlation of core segments according to geocemical and optical infromation, the resulting 17.7 m composite core was continuously sampled at 2-cm-resolution, yielding a total of 849 samples. It is comprised of three major lithofacies, which differ in colour, sediment structure, grain size, organic-matter and carbonate content, and geochemistry. There are no lithological indications of any hiatuses or instances of non-contiguous sedimentation in core Co1215. A detailed lithostratigraphic characterisation of the entire succession (90–0 ka) is presented in Damaschke et al. (2013), along with details of the six visible tephra layers and five cryptotephra layers identified in Co1215 (**Table S1**).

Published data for Lake Prespa (Co1215) includes: total carbon (TC), total inorganic carbon (TIC), and total sulphur (TS) analyses (Aufgebauer et al., 2012; Damaschke et al., 2013). These data were measured at ~2 cm resolution with a DIMATOC 200 (DIMATEC Co., Germany), and TS using a Vario Micro Cube combustion CNS elemental analyser (VARIO Co.) at the University of Cologne. TOC was calculated as the difference between TC and TIC by Aufgebauer et al. (2012) for the upper ~3.2 m, and by Damaschke el a. (2013) for the full ~17 m succession ~~(Aufgebauer et al., 2012; Damaschke et al., 2013)~~. The inorganic chemistry of the sediments was determined by X-ray fluorescence (XRF) data, generated using an ITRAX core scanner (COX Ltd., Sweden) equipped with a Mo-tube set to 30 kV and 30 mA, and a Si-drift chamber detector (Wagner et al., 2012). Core Co1215 was scanned with a resolution of 2 mm and a scanning time of 10 seconds per measurement. Elemental intensities were obtained for potassium (K), titanium (Ti), manganese (Mn), strontium (Sr), iron (Fe), calcium (Ca), and rubidium (Rb) (Wagner et al., 2012).

### 3.1.1. Chronology

A chronology for Co1215 was previously produced by linear interpolation using volcanic ash layers, coupled with $^{14}$C and electron spin resonance (ESR) dates obtained for bulk organic, fish, and aquatic plant remains (Aufgebauer et al., 2012). Here, we update this chronology with a Bayesian age-depth

model that re-calculates previously obtained $^{14}$C-dates (**Table S2**) with the latest (Intcal2020) radiocarbon calibration (**Fig. 3**) (Reimer et al., 2020). We used rBacon v 2.5.7 (Blaauw and Christen, 2011), and the new age model includes updated $^{40}$Ar/$^{39}$Ar dates of two eruptions geochemically correlated to specific tephra layers within the Prespa core (Damaschke et al., 2013); the Y-5 (39.85 ± 0.14 ka , 2σ (Giaccio et al., 2017)) and Y-6 (45.50 ± 1 ka, 2σ (Zanchetta et al., 2018; Scaillet et al., 2013)) tephra units. ~~Each~~ Every tephra layer is ~~assumed~~ to have been deposited instantaneously. The final model used herein presents the median of all the iterations (generally indistinguishable from the mean), and when referring to ages of specific depths within the core we include the 95% confidence intervals. The upper 2 m (Holocene) section of core Co1215 is chronologically well constrained by 10 $^{14}$C dates and two tephra layers, with modelled age uncertainties in this section ranging from ~5 to 580 years. Uncertainty increases with depth due to the lack of independent chronological anchors available. For example, three ESR dates for a shell fragment layer (~14.6 m depth) give an average age of 73.6 ± 7.7 ka, and form the only tie point currently available below 8.5 m ~~depth~~. All twenty-seven tie-points and accompanying chronological details are presented in **Text SI3** and **Table S3~~1~~**. Our revised model shows broad agreement with the interpolation-based chronology presented by Damaschke et al. (2013), and ~~confirms~~ suggests that core Co1215 provides a continuous record of sedimentation over the past ~90-kyr (**Fig. S1**), with each 2 cm sample equating to ~100 years (on average).

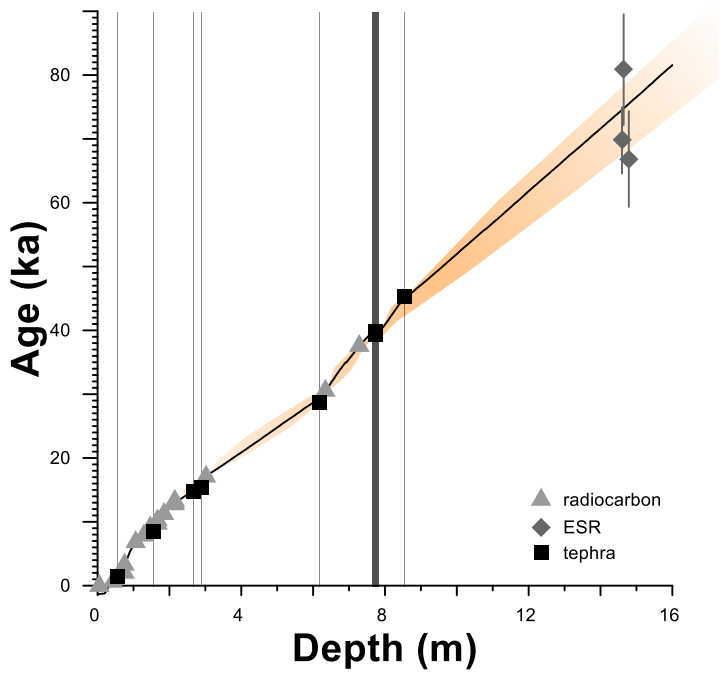


**Figure 3**: A Bayesian age-depth model for core Co1215 from Lake Prespa. Calibrated ages for the twenty-seven tie points used in model generation are displayed by type: radiocarbon-dated bulk organic, fish, or aquatic plant remains (light grey triangles), volcanic tephra layers (black squares) and electron-spin resonance (ESR)-derived dates for a shell layer (*Dreissena*) located at 14.63–14.58 m depth (dark grey diamonds). Uncertainties for ESR dates at 1σ are presented as dark grey vertical lines. Black line marks the median core age predicted by the model, which is generally indistinguishable from the predicted mean. Minimum and maximum model ages at 95% (2σ) confidence are marked with orange shading. Grey bars mark the stratigraphic placement of tephra layers used as tie-points, and widths of these bars are proportional to the thickness of the tephra layers within the core, respectively. Uncertainties for radiocarbon and tephra dates are within the displayed point sizes, and presented in **Table S4**.

## 3.2. Lake Ohrid (core 5045-1)

The 5045-1 coring site ("DEEP") is located in the central part of Lake Ohrid (41°02'57" N, 20°42'54" E) (**Fig. 2**). The uppermost 1.5 m of sediments at DEEP were recovered in 2011 using a UWITEC gravity and piston corer. Sediments below 1.5 m depth were recovered from six closely-spaced drill holes at the site in 2013 (5045-1A to 5045-1F), with a total composite field recovery amounting to > 95% (545 m); accounting for overlap between cores (Wagner et al., 2014b). ~~In 2013, sediments below 1.5 m depth were recovered from six closely-spaced drill holes at the site (5045-1A to 5045-1F (Francke et al., 2016)).~~ Sediment cores were spliced to a composite record using optical and geochemical information. For sedimentological and geochemical analyses, 2 cm thick slices (40.7 $cm^3$) were removed from the core at a resolution of 16 cm (~480-yr) at the University of Cologne. For this study, we analysed 217 samples from between 0 and 36.27 m composite depth. We cannot entirely rule out that changes in sedimentation occurred between samples, however, recent seismic (Lindhorst et al., 2015), borehole logging (Ulfers et al., 2022) and sedimentological studies (Wagner et al., 2022, 2019) suggest that sedimentation at the DEEP site has been near-continuous since ~1.3 Ma, with no clear evidence for any major (>1-kyr) hiatuses. A detailed lithostratigraphic characterisation of the 5045-1 core succession is presented by Francke et al. (2016). Details of the six microscopic and two visible tephra layers identified in the ~36 m section analysed in this study are presented by Leicher et al. (2021), and listed in **Table S3**.

The Hg data obtained from core ~~Lake Ohrid~~ (5045-1) ~~Hg data~~are presented herein ~~are paired with two~~alongside previously existing datasets. The first dataset comprises TC and TIC measured using a DIMATOC 200 (TOC calculated as the difference between TC and TIC), and TS using a Vario Micro Cube combustion CNS elemental analyser at the University of Cologne ~~by~~ – both by Francke et al. (2016). ~~TOC was calculated as the difference between TC and TIC (Francke et al., 2016; Wagner et al., 2019).~~ The second dataset comprises XRF data using an ITRAX XRF core scanner at the University of Cologne at 2.56 m increments carried out on 2 cm thick samples, and processed using QSpec 6.5 software (Cox Analytical, Sweden) by Francke et al. (2016). Elemental intensities were obtained for K, Ti, Fe, ~~zirconium (~~Zr~~)~~, and Ca ~~(Francke et al., 2016; Wagner et al., 2019)~~. To validate the quality of the XRF scanning data, conventional wavelength dispersive XRF (WDXRF, Philips PW 2400, Panalytical Cor., the Netherlands) was conducted on the 2-cm-thick samples at 2.56-m resolution. ITRAX data for each 2-cm-thick WDXRF sample was averaged to ensure comparability with the conventional XRF data, and $r^2$ values were to compare ITRAX and WDXRX datasets (~~full analytical details in~~ Francke et al. (2016)).

### 3.2.1. Chronology

This study uses the age-depth model generated by Francke et al. (2016), and extended by Wagner et al. (2019) for the upper ~248 m and ~447 m of core 5045-1, respectively. Both combined

tephrochronological data with orbital parameters using a Bayesian age modelling approach (Bacon 2.2~~69~~). Tephra layers were used as first-order constraints. From the eleven total $^{39}Ar/^{40}Ar$ dated tephra layers employed in Wagner et al. (2019), seven are found in the upper ~36 m section analysed in this study ~~(**Table S4**)~~. The age of the eighth tie-point (OH-DP-0009) is defined following geochemical correlation of this tephra layer to the AD472/512 eruption of Somma-Vesuvius, Italy (Francke et al., 2019; Leicher et al., 2021). This chronological information was coupled with climate-sensitive proxy data (TOC and TIC) to define cross-correlation/inflection points with orbital parameters, which were included in the age–depth model as second-order constraints (**Table S~~4~~6**). Four of these points correspond to the ~36 m interval analysed in this study (Wagner et al., 2019). The 95% confidence intervals of ages for specific depths produced by the model average at ±5.5 kyr, with a maximum of ±10.6 kyr. The resulting chronology suggests that the 0.97-36.27 m core section analysed here covers the time interval 1.6 – 89.6 ka, with each sample possessing a resolution of ~400 years (Francke et al., 2016; Wagner et al., 2019). Full description of the 5045-1 chronology and associated methods are presented in **Supplementary Text SI4.**

## 3.3. Mercury measurements

Total Hg concentrations ($Hg_T$) in the bulk sediments of cores 5045-1 (Ohrid) and Co1215 (Prespa) were measured using an RA-915 Plus Portable Mercury Analyzer with PYRO-915 Pyrolyzer, Lumex (Bin et al., 2001) at the University of Oxford. Samples were analysed for $Hg_T$ at a resolution of ~2 cm for Co1215 (Lake Prespa), and ~16 cm for 5045-1 (Lake Ohrid) (see sections **3.1** and **3.2**). Approximately 2 $cm^3$ of sediment was homogenized to fine powder for TOC (Wagner et al., 2019; Francke et al., 2016; Aufgebauer et al., 2012a; Damaschke et al., 2013) and Hg analyses (this study). For Hg analysis, ~~P~~powdered samples were weighed into glass measuring boats, with masses ranging between 35–96 mg for Co1215, and between 27–78 mg for 5045-1. For samples particularly rich in inorganic fractions (e.g., samples coinciding with tephra layers), masses needed to be greater in order to yield a sufficiently high peak area (Lumex output) for calculation of sediment mercury concentrations. Samples were then placed into the pyrolyzer (Mode 1) and heated to ~700°C, volatilizing any Hg in the sample. Spectral analysis of the gases produced yields the total Hg content of the sample. Six measures of standard material (paint-contaminated soil – NIST Standard Reference Material ® 2587) with an expected Hg concentration of 290 ± 9 ng $g^{-1}$ (95% confidence) were run to calibrate the instrument prior to sample analysis, and then one standard between every 10 lacustrine samples ~~with a known Hg value of 290 ng $g^{-1}$ were run to calibrate the instrument prior to sample analysis, and then one standard for every 10 lacustrine samples~~ (calibration results in **Supplementary Information**). Long-term observations of standard measurements with total Hg yield similar to the sediment samples analysed here indicate reproducibility is ± 6~~10~~% or better for Hg concentrations >10 ng $g^{-1}$ (Frieling et al., 2023), and with Hg recovery close to 100% as expected from pyrolysis-based instrumentation (Bin et al., 2001). Details of standard runs for each core are included as a supplementary file.~~.~~

### 3.3.1. Mercury accumulation

Rates of Hg accumulation in both cores were calculated by:

$$Hg_{AR} = Hg_T (DBD \times SR) \quad \text{(eqn. 1)}$$

where $Hg_{AR}$ is the total Hg mass accumulation rate (mg $m^{-2}$ $kyr^{-1}$), $Hg_T$ is the total mercury concentration (expressed in mg $g^{-1}$), DBD is the dry bulk density (g $m^{-3}$), and SR is the sedimentation rate (SR) in ~~(~~m $kyr^{-1}$~~)~~. Values for $Hg_{AR}$ are also calculated with respect to the median age estimate for each sample, meaning that uncertainties increase with depth.

Sedimentation rate rates for both Prespa and Ohrid were calculated by combining stratigraphic and lithological observations with the age-depth relationship ascertained for each core, respectively. For Lake Prespa, we calculate the sedimentation rate using the updated age-depth model presented in **section 3.1.2**. Dry bulk density values were calculated on the basis of sedimentological data available for each core. For the Lake Ohrid dataset, DBD values were already available following the analyses of Francke et al. (2016). To acquire these values for Lake Prespa, we employed the formula:

~~For Lake Prespa, we calculate the sedimentation rate using the updated age model presented in **section 3.1.2**. To calculate DBD, we employed the formula:~~

$$DBD = M_{solid} / V_{total} \quad \text{(eqn. 2)}$$

where $M_{solid}$ is the mass of dry solid material (g) measured in each sample, and $V_{total}$ is the volume of each respective sample (2 $cm^3$). Values for $M_{solid}$ were calculated based on recorded weight loss between wet and dry samples taken for CNS analyses by Aufgebauer et al. (2012), assuming an average wet density of 1 g $cm^{-3}$ for wet sediments, and 2.6 g $cm^{-3}$ (grain density) for dry sediments.~~.~~

For Lake Ohrid, we utilise the sedimentation rate values calculated by Wagner et al. (2019), and dry bulk density measurements measured by Francke et al. (2016) (see these publications for full methods).

## 3.4. Mercury normalization

The availability of specific host phases is often assumed to exert control on the sedimentary burial of Hg. Here, we test if the Hg deposited into the sediments of lakes Prespa and Ohrid may be impacted by abundance of a suite of phases. To do this, we assess both $Hg_T$ records relative to quantitative estimates of TOC and TS (assuming sulphides contribute to TS): both considered potential host phases of Hg in sedimentary successions (Chakraborty et al., 2015; Garcia-Ordiales et al., 2018; Ravichandran, 2004; Shen et al., 2020).

Detrital minerals constitute another potential host phase of Hg in sedimentary records. Elements such as Al, Ti, K, Zr, and Rb are commonly used as proxies for this purpose (Kongchum et al., 2011;

Percival et al., 2018b; Shen et al., 2020). We observe a close correlation between K and Ti in Lake Prespa, and quartz in Lake Ohrid (**Fig. S2**): all proxies for fine-grained material inputs to a lake basin (Grygar et al., 2019; Warrier et al., 2016). To facilitate direct comparison of the two cores, we assess the relative abundances of (fine-grained) detrital material using XRF-based K counts. To account for differences in resolution between Hg and XRF data, K measurements were averaged to the thickness of each discrete Hg sample, and K values corresponding to the Hg sample depths extracted.

In line with previous studies (Shen et al., 2020), we assume that the strongest positive-sloped linear correlation with Hg among the analysed elements TS, TOC, and K signals the most likely dominant influence on Hg loading in each core, which may then be interpreted as the 'host-phase'. However, it is conceivable that different host phases may dominate in different sections of the individual cores or that no single host-phase clearly dominates, and so the same approach is also applied restricted to the data within each individual marine isotope stage (MIS) (**Table 1**).

# 4. Results & Discussion

Sediment cores extracted from Lake Prespa (Co1215) and Lake Ohrid (5045-1) provide a detailed, time-resolved record of Hg cycling between ~90 and 0 ka. Results are presented with direct reference to key stratigraphic intervals: the Holocene (12–0 ka; MIS 1), and the late Pleistocene (120 –12 ka; MIS 2–5). Widespread proxy-based evidence for warmer temperatures, forest expansion, and increased precipitation representative of ~~Evidence for~~ interglacial climatic conditions marks the start of the Holocene epoch (~12 ka) in SE Europe (Kern et al., 2022; Panagiotopoulos et al., 2014; Sadori et al., 2016; Tzedakis et al., 2006). For simplicity, we hereafter equate "MIS 1" to the Holocene, allowing a clearer distinction between glacial (late Pleistocene) and interglacial (Holocene) climate conditions. We use these time-slices, that also represent broad climate and environmental 'modes', as a framework upon which the Hg composition of both cores can be directly compared relative to local changes in sediment lithology and geochemistry (**Table 1**), and a foundation upon which local and regional-scale environmental changes can be assessed relative to global shifts in glaciation, climate, sea level, and ocean circulation. We first consider the extent to which soft sediment processes (**section 4.1**) and lithological features (**section 4.2**.) may have influenced the Hg variability observed in **Figures 5** and **6**, before adopting a catchment-scale perspective in **section 4.3** to explore the role of diverse environmental processes in Hg cycling through these two systems.

**Table 1**: A comparison of the features of cores Co1215 (Lake Prespa) and 5045-1 (Lake Ohrid) relative to the late Pleistocene (LP; 120 – 12 ka), the Holocene (H; 12 – 0 ka), and the marine isotope stage (MIS) stratigraphic framework defined in Lisiecki & Raymo (2005)*. $Hg_T$ is given in ng $g^{-1}$, and $Hg_{AR}$ is given in mg $m^{-2}$ $kyr^{-1}$.

| | | | Depth (m) | Mean | | Sedimentology** | |
|---|---|---|---|---|---|---|---|
| | | | | $Hg_T$ | $Hg_{AR}$ | Lithology | Key Features |
| Lake Prespa | Holocene | MIS 1 | 2.4–0 | 64.6 | 34.7 | Silt gyttja. Decreasing sand content with depth. | High lake levels. One visible and one microscopic tephra layer. High microcharcoal and green algae concentrations. High TOC/TN ratios. High sedimentation rate. |
| | Late Pleistocene | MIS 2 | 6–2.4 | 41.9 | 16.4 | **2.9–2.4 m** – High fine sand (<250 µm), with clayey silt and evidence of lamination. | Increasing lake level. Two cryptotephra layers. Transient nutrient pulse 12.8–11.7 ka. Moderate TOC and low TIC. |
| | | | | | | **6–2.9 m** – Homogenous sediment structure. Silt, distinct lamination and siderite precipitation. | Evidence for ice-rafted debris deposition. Low productivity and lake level. High K and organic $\delta^{13}C$. Low water $\delta^{18}O$. Declining C/N ratios. High sedimentation rate. |
| | | MIS 3 | 11–6.1 | 32.8 | 8.9 | **6.6–6.1 m** - Massive sediment structure. Silt with distinct lamination. | Steady decrease in lake level. High oxygen index. |
| | | | | | | **11–6.6 m** – Massive sediment structure. Silt. | Increasing lake level. Four visible and three microscopic tephra layers. High C/N ratios. Moderate TOC, very low TIC. |
| | | MIS 4 | 13.9–11 | 33.7 | 10.4 | Massive sediment structure. Clayey silt. | High sedimentation rate. Very low TOC. No tephra layers. Low productivity. Declining C/N ratios. High K content gives evidence for ice-rafted debris deposition. |
| | | MIS 5a-c | 17.7–13.9 | 44.2 | 13.3 | **15.2–13.9 m** - Massive, bioturbated sediments. Clayey silt and fine sand. | Increasing lake level and high productivity. *Dreissena* shell layer 14.58–14.56 m. |
| | | | | | | **17.8–15.2 m** – Massive sediment structure. Clayey silt with fine sand (a). | Deep lake with moderate/low productivity High green algae concentrations. High TOC, low TIC. |
| Lake Ohrid | Holocene | MIS 1 | 4.6 – 1.1 | 47.2 | 26.2 | **3–0 m** – Massive sediment structure. Bright colouring indicates high calcite; dark colouring indicates lower calcite. | High productivity. Four microscopic tephra layers. Low K concentrations. High sedimentation rate. |
| | | | | | | **4.6–3 m** – Slightly calcareous silty clay and massive sediment structure. Frequent siderite-rich layers. | Low TIC and calcite. High iron availability. Low productivity and stronger calcite dissolution. High K concentrations. High sedimentation rate. |
| | Late Pleistocene | MIS 2 | 11.3 – 4.6 | 69.2 | 45.5 | Silty clay. Mottled, often massive sediment structure. Frequent siderite-rich layers. Abundant fine fraction (< 4 µm) sediments. | Very low TIC, TOC, and calcite suggesting low productivity, with large inputs of fine-grained, and chemically weathered siliciclastics. High iron availability. Two visible and two microscopic tephra layers. Mass-movement deposit at 7.87 m. |
| | | MIS 3 | 23–11.3 | 50.6 | 33.4 | | |
| | | MIS 4 | 28.8–23 | 50.2 | 29.6 | | |
| | | MIS 5a-c | 36.3–28.8 | 36 | 20.4 | **35.6 – 28.8 m** – Silty clay with a massive sediment structure. Bright colouring indicates high calcite; dark colouring indicates lower calcite. | Low siliciclastic mineral abundance. Decreasing $\delta^{18}O$ and $\delta^{13}C$. Strong primary productivity. Low sedimentation rate. |
| | | | | | | **36.6 – 35.6 m** – Silty clay. Mottled, often massive sediment structure. Frequent siderite-rich layers. | Higher carbonate $\delta^{18}O$ and $\delta^{13}C$ corresponds to reduced TIC, and high siderite. Low sedimentation rate. |

* MIS 5a-c – 96–71 ka; MIS 4 – 71–57 ka; MIS 3 – 57–29 ka; MIS 2 – 29–12 ka; MIS 1 – 12–0 ka.

**Summarised from the following references:

**Lake Prespa** - (Aufgebauer et al., 2012; Cvetkoska et al., 2015; Damaschke et al., 2013; Leng et al., 2013; Panagiotopoulos et al., 2014; Wagner et al., 2014)

**Lake Ohrid** - (Francke et al., 2016, 2019; Just et al., 2015; Lacey et al., 2016; Leicher et al., 2021; Wagner et al., 2019)

## 4.1. Host Phase Controls

The availability and abundance of specific host phases is often assumed to control sedimentary Hg accumulation and burial (Outridge et al., 2007). Both Lake Prespa and Lake Ohrid show evidence for complex relationships between $Hg_T$, TOC, TS, and K concentrations through time (**Fig. 4**). However, the trends displayed in **Figure 4** also suggest that: (1) the strength of the relationships between Hg, TOC, TS, and detrital minerals (K) are distinctly different between the two lakes, and (2) the $Hg_T$ signals preserved in Lake Prespa and Lake Ohrid cannot be fully explained by variability in abundance of these potential host phases individually.

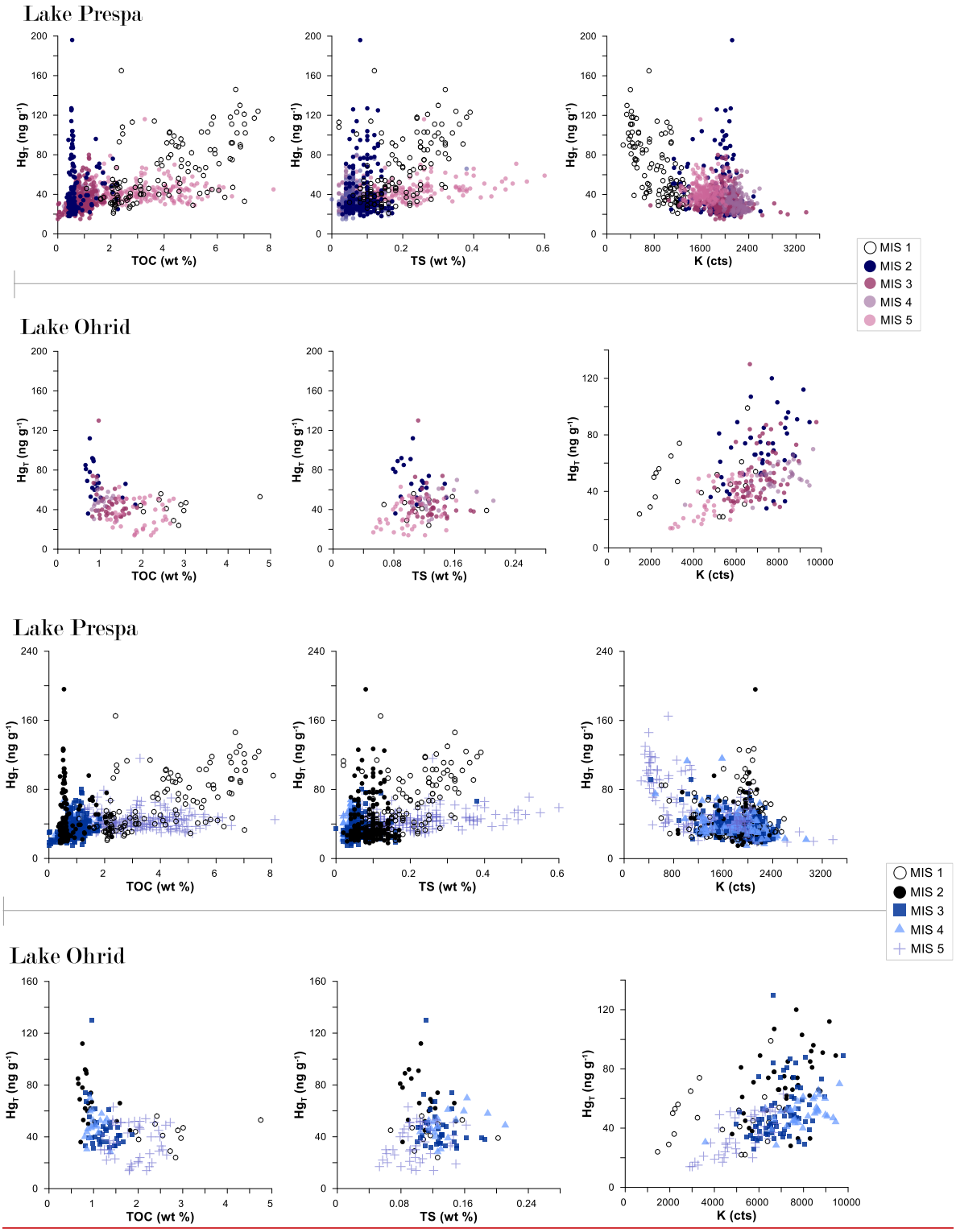


**Figure 4**: A comparison of host-phase relationships between lakes Prespa and Ohrid. Points are colour-coded relative to stratigraphic period: the Holocene (12–0 ka, transparent circles), and the late Pleistocene (90–12 ka, filled symbols~~filled circles~~). We compare $Hg_T$ records for both lakes relative to total organic carbon (TOC), sulphide (estimated by total sulphur (TS)), and detrital minerals (estimated by potassium (K) concentrations) – note that aluminium (Al) data are more commonly used as an indicator of detrital mineral abundance but these are currently unavailable for 5045-1.

436

Core Co1215 from Lake Prespa shows a moderate correlation between $Hg_T$ and TOC during the Holocene and late Pleistocene (all data in **Fig. 4; Table 1**). This correlation is most significant during the Holocene (MIS 1), where distinct enrichments in $Hg_T$ occur in conjunction with a similarly sharp increase in TOC, and low variability in Hg/TOC values (**Fig. 5**). However, it is more inconsistent during the late Pleistocene (MIS 2–5). For example, the highest $Hg_T$ values are measured in the relatively TOC-lean sediments of MIS 2 (**Fig. 4, 5**), and a plateau also appears when higher TOC concentrations are reached during MIS 5 whereby $Hg_T$ no longer increased in step with TOC (**Fig. 4, S2**). The correlations observed are not strong enough to conclude that TOC availability can fully explain the Hg signals observed in Lake Prespa throughout the 90-kyr succession.

Correlations between $Hg_T$, detrital mineral and/or TS availability are also largely absent, suggesting that the complex Hg/TOC relationship is not a function of time-varying sulphides and detrital mineral availability. Large peaks in Hg/K are visible during the Holocene (**Fig. 5**), but these are not reflected in $Hg_{AR}$ and therefore an artefact of considerably lower K concentrations within this section of the core rather than indicators of changes in lake Hg levels. The highest positive $r^2$ value between $Hg_T$ and TS is observed during the Holocene (MIS 1: $r^2 = 0.25$) (**Fig. 4**), implying that >75 % of variance in the dataset cannot be explained with sulphide availability during this time period. Correlations for other periods are even weaker and some periods appear to show distinct patterns of Hg and potential host-phase behaviour (**Fig. 4**).

One possibility is that Hg signals reflect changes in the dominant sources of organic and detrital materials deposited in the lake. For example, combined isotopic and sedimentological data record episodes of stronger algal blooms during MIS 1 and 5 (Leng et al., 2013), supported by coeval abundance of freshwater diatom genera such as *Cyclotella* and *Aulacoseira* (Cvetkoska et al., 2015). All correspond to elevated $Hg_T$, and so could imply more effective Hg burial by autochthonous organic material compared to allochthonous (Leng et al., 2013; Damaschke et al., 2013). However, in the presence of abundant binding ligands such as for the Lake Prespa record, maximum Hg burial is limited principally by supply regardless of productivity, and so changing Hg signals in Lake Prespa more likely reflect changes in environmental Hg availability; resulting from externally-driven oscillations in Hg emission and/or exchange between (local) surface reservoirs such as forests, water courses, and soils (Bishop et al., 2020; Obrist et al., 2018)). This interpretation is supported by the lack of a close statistical correspondence between Hg, organic matter, sulphur, or detrital mineral content, source, or composition (**Fig. 4**), which suggests that Hg burial efficiency is only weakly associated with host phase availability in this system.

~~This could imply that our Hg data captures: (1) catchment-driven shifts in sources of organic matter and detrital material deposited into the lake (Leng et al., 2013), and/or (2) significant changes in the overall availability of Hg in the environment through time (e.g., due to a change in rates of Hg emission and/or exchange between (local) surface reservoirs (Bishop et al., 2020)). Nonetheless, Hg variability in the Prespa Hg dataset cannot be fully explained by changes in organic matter, sulphur, or detrital mineral content (**Fig. 4**), implying that Hg flux, rather than host phase availability, controls Hg sequestration in Lake Prespa.~~

476

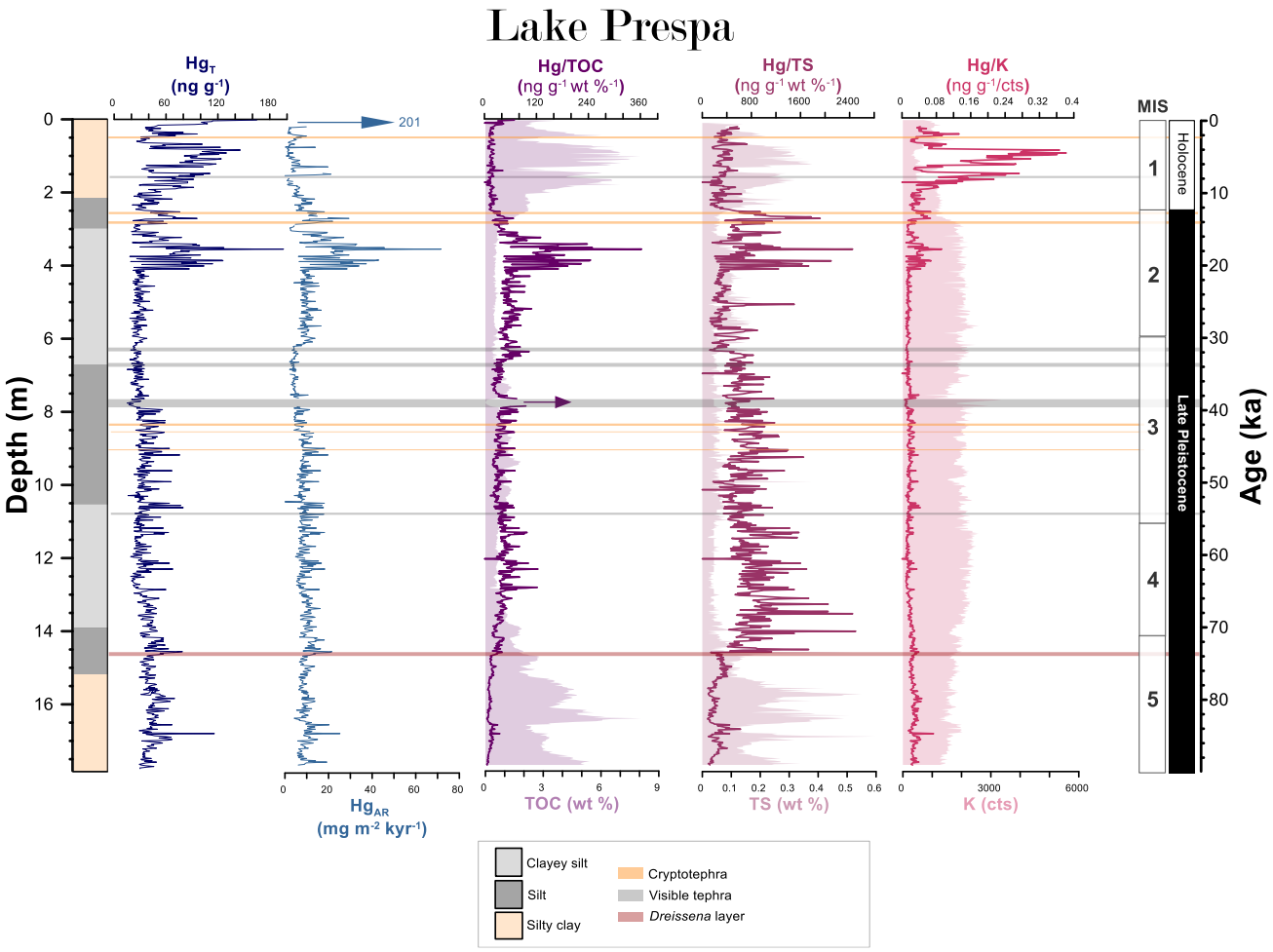


**Figure 5**: Total Hg ($Hg_T$) and total Hg accumulation rate ($Hg_{AR}$) for core Co1215 from Lake Prespa, presented as a function of depth and time, and relative to lithofacies, visible (grey shading) and cryptotephra (orange shading) layers. We include records of $Hg_T$ (this study) normalized to records of total organic carbon (TOC) (Damaschke et al., 2013), ~~sulphide (estimated by~~ total sulphur (TS)~~)~~ (Aufgebauer et al., 2012), and detrital mineral abundance (estimated by potassium (K)) (Panagiotopoulos et al., 2014), with filled shading marking the original datasets. A distinct lake low stand based on seismic profiles and sedimentological data is marked at 14.63 - 14.58 m depth (red shading) (Wagner et al., 2014a). A purple arrow marks sections where artificially high Hg/TOC values are generated by a sharp drop to near-zero TOC (<0.06 wt %) coinciding with deposition of the Y-5 (17.1 m) tephra unit – an effect expected as background sedimentation is interrupted by volcanic ash deposition. White boxes mark the marine isotope stages defined by (Lisiecki and Raymo, 2005), and stratigraphic periods are labelled in black/white.

477

478 Core 5045-1 from Lake Ohrid shows elevated $Hg_T$ during the late Pleistocene compared to the
479 Holocene (**Fig. 6; Table 1**). Peaks in $Hg_T$ most consistently correspond to increases in K (detrital
480 mineral) intensities, reflected in a broadly positive relationship between $Hg_T$ and K throughout the
481 succession (**Fig. 4, S3**). However, this relationship is only described by $r^2$ values <0.5 and the
482 strength of this correlation varies across the span of the record, weakening during the Holocene (**Fig.**
483 **4**)~~.~~.

484 Variable Hg values in the Ohrid record appear less influenced by organic matter and/or sulphide
485 availability. Fluctuations in TOC/TS values suggest that some sulphide formation may have occurred
486 during the late Pleistocene (MIS 2-5) (Wagner et al., 2009; Francke et al., 2016). However, even in

these phases, TS remains low and correlations between $Hg_T$ and TS are generally negative or weak ($r^2 < 0.2$; **Fig. 4**) so that Hg signals do not change in magnitude or expression even when TS variability is accounted for (**Fig. 6**), potentially due to the oligotrophic state of Lake Ohrid favouring burial of sulphide-depleted sediments (Francke et al., 2016; Vogel et al., 2010). More remarkable, the relationship between $Hg_T$ and organic matter in Lake Ohrid also shows an inverse correlation (**Fig. 4**). ~~somewhat reminiscent of a trend observed in the uppermost sediments of a ~5 Ma succession from Lake Baikal (Russia) (Gelety et al., 2007).~~ These trends may be explained by a scenario where the Hg flux to Ohrid from direct deposition and/or surrounding catchment is typically the limiting factor, rather than availability of potential host phases.

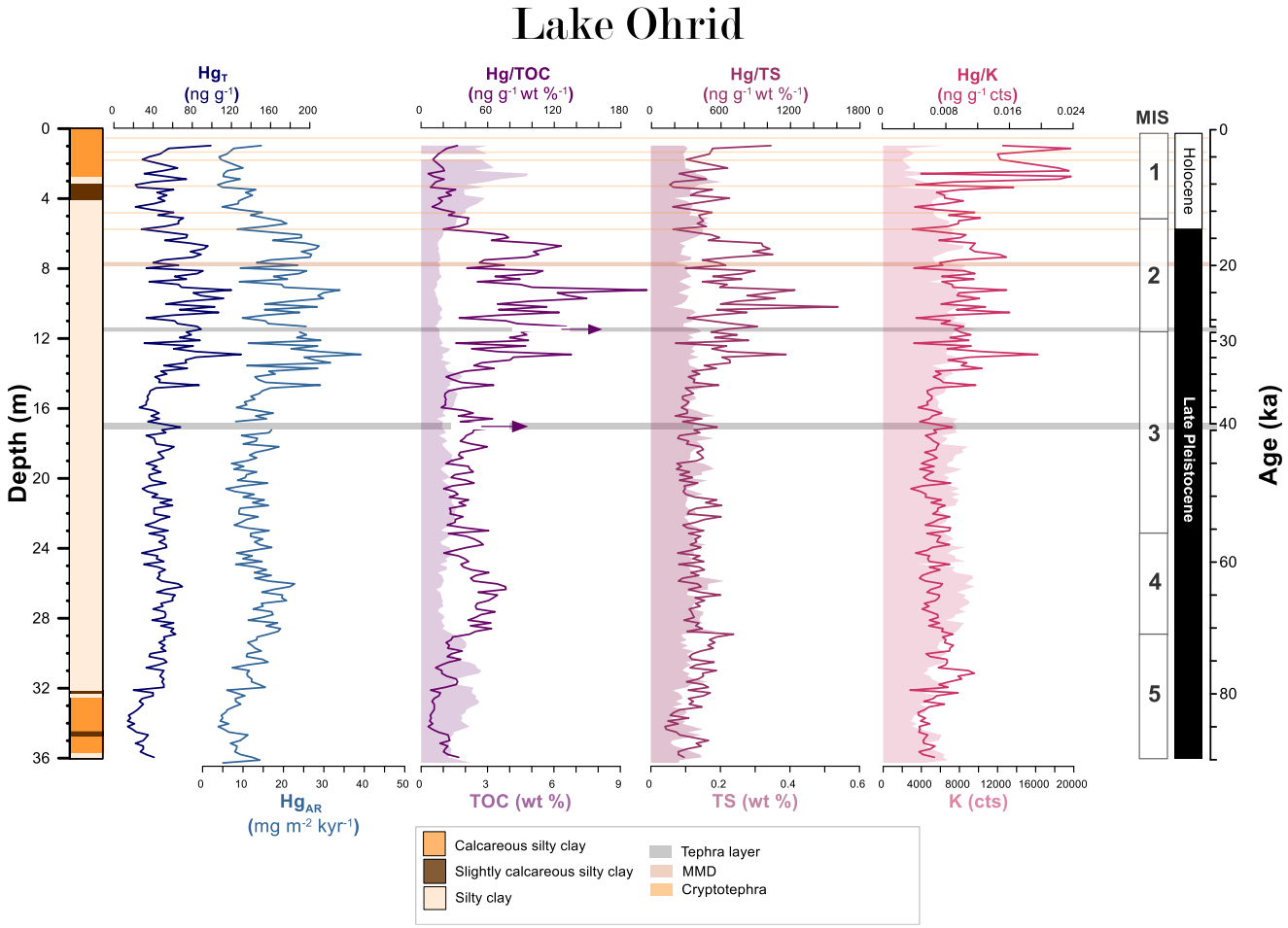


**Figure 6**: Total Hg ($Hg_T$) and total Hg accumulation rate ($Hg_{AR}$) for core 5045-1 from Lake Ohrid, presented as a function of depth and time, and relative to lithofacies, visible (grey shading) and cryptotephra (orange shading) layers. We include records of $Hg_T$ (this study) normalized to records of total organic carbon (TOC) (Francke et al., 2016), sulphide (estimated by total sulphur (TS)) (Francke et al., 2016), and detrital mineral abundance (estimated by potassium (K)) (Francke et al., 2016; Wagner et al., 2019), with filled shading marking the original datasets. A mass movement deposit (MMD) is marked at 7.87 m depth (brown shading) (Francke et al., 2016). Purple arrows mark sections where artificially high Hg/TOC values are generated by a sharp drop to near-zero TOC (<0.06 wt %) coinciding with deposition of the Y-5 (17.1 m) and Mercato (11.5 m) tephra layers – an effect expected as background sedimentation is interrupted by volcanic ash deposition. White boxes mark the marine isotope stages as defined by Lisiecki and Raymo (2005), and stratigraphic periods are labelled in black/white.

Lake Ohrid and Lake Prespa show distinct differences in the strength of their Hg-host phase relationships. In Lake Prespa, Hg broadly covaries with organic matter (TOC), whereas in Lake Ohrid correlations are observed between Hg and detrital minerals (K). Nonetheless, only a relatively small

proportion of Hg variability can be explained by host phase availability in each record. This suggests that while host phase availability may, at times, exert an influence on the Hg signals recorded in these lakes, the catchment-controlled changes in Hg fluxes are typically the more dominant effect on Hg in these sediment records. In the absence of a pronounced host-phase influence, retention of a measurable Hg signal requires that the net influx of Hg into the lake (e.g., surface runoff, wet/dry deposition) exceeds the amount leaving the system due to processes such as runoff or evasion. Therefore, we surmise that the $Hg_T$ and $Hg_{AR}$ signals recorded in Lake Prespa and Lake Ohrid are records of net Hg input to the two lakes rather than the efficiency of sedimentary drawdown.~~We therefore surmise that the $Hg_T$ and $Hg_{AR}$ signals recorded in Lake Prespa and Lake Ohrid are records of net Hg input to the two lakes rather than the efficiency of sedimentary drawdown.~~

## 4.2. Tephra layers

As volcanic eruptions are among the most significant natural Hg sources, we assess whether the previously recognized tephra deposition events in Lake Prespa correspond to changes in Hg deposition. Overall, we find that individual tephra horizons and surrounding sediments do not consistently correspond to measurable peaks in $Hg_T$ or $Hg_{AR}$ in Lake Prespa (**Fig. 5**). ~~Despite a resolution of <100-years per sample, o~~Only two of the eleven preserved ash layers coincide with elevated $Hg_T$: Mercato (8.54 ± 0.09 ka; Somma-Vesuvius), and LN1 (14.75 ± 0.52 ka; Campi Flegrei). These two units are not associated with disproportionately large tephra volumes and neither coincide with evidence for transient changes in authigenic carbonate precipitation or sediment diagenesis that may impact sedimentary Hg. This implies that Hg concentrations in Lake Prespa cannot, in general, be unequivocally linked to short-lived (<1-year) individual eruption events between ~90 and 0 ka (**Fig. S5**).

Discrete ash fall events (recorded by tephra/cryptotephra) do not consistently correspond to measurable peaks in $Hg_T$ or $Hg_{AR}$ in the slightly lower-resolution (~400-yr per sample) Lake Ohrid record (**Fig. S5**). Considering this lack of correspondence of Hg with ash layers, in conjunction with the Lake Prespa data too, suggests that (a) surface Hg loading was not appreciably increased with most large eruption events over the past 90 kyr in the Balkans and/or (b) sampling resolution may need to be significantly higher and/or focused on lesser-bioturbated records to identify single, short-lived volcanogenic perturbations of the scale and type occurring during the period recorded in the Ohrid (and Prespa) sedimentary successions.

## 4.3. Variability through time

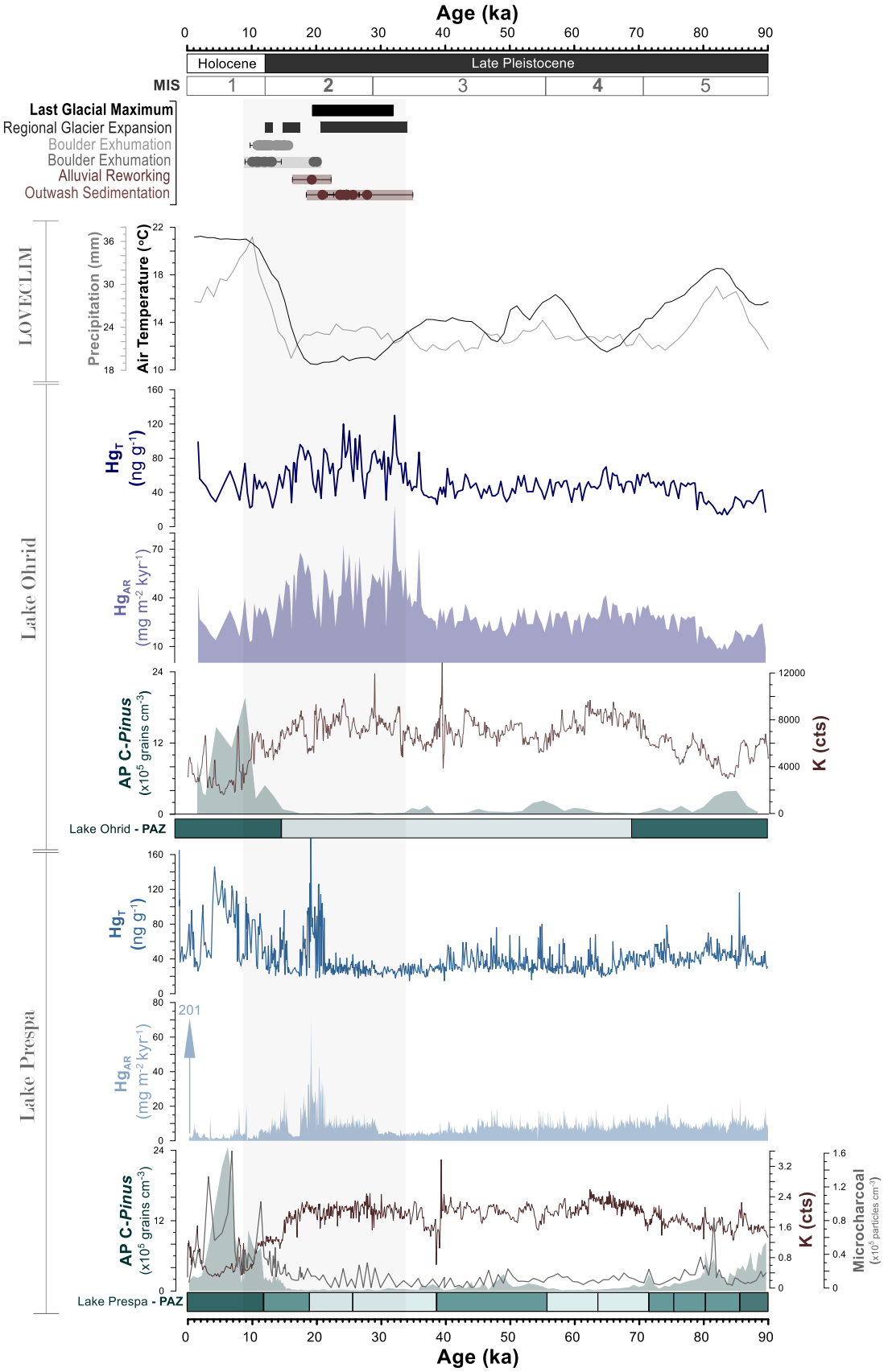

**Figure 7**: Total mercury ($Hg_T$) and mercury accumulation rate ($Hg_{AR}$) records for Lake Prespa and Lake Ohrid generated by this study and proxy datasets generated by prior studies. For Lake Prespa, these include arboreal pollen (AP) concentrations (Panagiotopoulos et al., 2014), microcharcoal (Panagiotopoulos, 2013), potassium (K) (Aufgebauer et al., 2012; Wagner et al., 2010), and pollen assemblage zones (PAZ) (Panagiotopoulos et al., 2014). For Lake Ohrid, these include AP concentrations (Sadori et al., 2016), potassium (K) (Wagner et al., 2019; Francke et al., 2016), 1000-year average surface-air temperature (SAT - °C) and annual mean precipitation (millimetres) both simulated by the LOVECLIM Earth system model (Goosse et al., 2010) for the Prespa/Ohrid region (Wagner et al., 2019), and pollen assemblage zones (PAZ) (Sadori et al., 2016). Pollen assemblage zones defined by Panagiotopoulos et al. (2014) (Lake Prespa) and Sadori et al. (2016) (Lake Ohrid) are presented as green bars, shaded relative to tree population density (darker colour = higher density). We include a chronology of glacial processes based on radiometric dating of glacial landforms in the following locations: the Voidomaitis river basin (purple) (Lewin et al., 1991; Woodward et al., 2008), the Pindus Mountains (lilac) (Allard et al., 2021, 2020; Styllas et al., 2018; Hughes et al., 2006; Pope et al., 2017), and the Dinaric Alps (blue) (Gromig et al., 2018; Ribolini et al., 2018; Ruszkiczay-Rüdiger et al., 2020). White boxes mark the marine isotope stages (MIS) as defined by Lisiecki and Raymo (2005), and stratigraphic periods are labelled in black/white. Vertical grey shading denotes the timing of the largest changes in glacier extent and volume.

### 4.3.1. Late Pleistocene (90 – 35 ka; MIS 5 to MIS3)

The Lake Prespa and Lake Ohrid sediment cores show similarly muted variability in $Hg_T$ and $Hg_{AR}$ values between ~90 and 35 ka (broadly MIS 5a-c, 4 & 3), alluding to relatively stable Hg inputs (**Fig. 7; Table 1**). High organic and low clastic material concentrations point to warmer climate conditions during this interval, in which both catchments experienced an increase in moisture availability, pronounced forest expansion, and plant diversification – collectively acting to stabilize hillslopes and reduce deep soil erosion (Francke et al., 2019; Panagiotopoulos et al., 2014; Sadori et al., 2016, 2016). One possibility is that Hg sequestration during this interval was controlled by consistent rates of algal scavenging (Biester et al., 2018; Outridge et al., 2007, 2019; Stern et al., 2009). Elevated TOC (**Fig. 5**), hydrogen index, TOC/TN, and biogenic carbonate concentrations between ~90 and 71 ka in both Lake Prespa and Lake Ohrid signal nutrient upwelling and increased allochthonous inputs, in conjunction with elevated primary productivity. For example, Lake Prespa records green algae accumulation (Cvetkoska et al., 2016, 2015; Leng et al., 2013; Panagiotopoulos et al., 2014), and sediments rich in biogenic silica ($bSiO_2$) are also ~~visible~~ evident in Lake Ohrid (Francke et al., 2016). Slow changes in lake geochemistry associated with these biological processes are consistent with a steady $Hg_{AR}$ in both Lake Prespa and Lake Ohrid during this time, and absence of any especially pronounced changes in $Hg_T$. This could suggest that, for a relatively prolonged period (~96–35 ka), Hg flux to the two lakes did not change with a magnitude sufficient to cause measurable sedimentary changes, and processes capable of amplifying differences in sedimentary Hg between Ohrid and Prespa were not particularly influential.

MIS 3 marks the start of slow divergence between the Hg records of Lake Prespa and Lake Ohrid. During MIS 3, proxy records suggest that conditions in the Prespa/Ohrid region were milder than MIS 4, but cooler and drier than MIS 5 (**Fig. 7**) (Panagiotopoulos et al., 2014; Sadori et al., 2016; Wagner et al., 2019). ~~Although often referred to as an 'interglacial', MIS 3 exhibits a distinctly more 'glacial' climate signature that is more comparable to MIS 4 in the Prespa/Ohrid region, for which proxy records point to a regional climate regime that was characterized by distinctly cooler, and also drier~~

~~climatic conditions (**Fig. 7**) (Panagiotopoulos et al., 2014; Sadori et al., 2016; Wagner et al., 2019).~~ Divergent Hg signals could be linked to two climate-driven processes. First, a reduction in primary productivity in Lake Prespa signalled by decreasing TOC, hydrogen index, and endogenic carbonate compared to values observed during MIS 5 (Aufgebauer et al., 2012; Cvetkoska et al., 2016; Leng et al., 2013). Second is an increase in detrital material flux to both lakes (signalled by elevated K count; **Fig. 7**), due to recession of the surrounding forests and subsequently elevated rates of catchment erosion (Damaschke et al., 2013; Francke et al., 2019; Panagiotopoulos et al., 2014; Sadori et al., 2016). This environmental shift is more likely to favour enhanced Hg mobility in the catchment and burial in a system whereby detrital minerals could either constitute the primary host phase or correlate to $Hg_T$; and so could explain the progressive elevation in $Hg_T$ and $Hg_{AR}$ observed in Lake Ohrid (**Fig. 4**).

### 4.3.2. Last Glaciation (35–12 ka; MIS 3 to MIS2)

The timing, amplitude, and expression of Hg signals captured in Lake Prespa and Lake Ohrid change significantly between ~35 and 12 ka (**Fig. 7**). The largest $Hg_T$ and $Hg_{AR}$ peaks in Lake Ohrid coincide with the Last Glacial Maximum (LGM), and begin at ~35 ka (**Fig. 7**). Synchronous enrichments in K, quartz, and Ti (Francke et al., 2016; Wagner et al., 2019) provide evidence for elevated clastic terrigenous matter inputs and erosion, and are consistent with evidence for a significantly less-vegetated catchment (Donders et al., 2021; Sadori et al., 2016). High clastic fluxes into the lake during the LGM could also relate to meltwater run-off from local mountain glaciers (Ribolini et al., 2011), which would transport large volumes of sediment generated by glacial abrasion, quarrying and plucking (Carrivick and Tweed, 2021; Overeem et al., 2017) into the lake basin. Given that Hg sequestration in Lake Ohrid appears partially related to the abundance of detrital minerals for much of the record (**Fig. 4, 5**), these Hg peaks could relate to local, climate-driven shifts in landscape structure associated with glaciation during MIS 2 (**Fig. 4, 7**).

Alternatively or in addition to these local effects, atmospheric mineral dust concentrations were also up to twenty-times higher during the LGM (Simonsen et al., 2019). Mineral dust may be the most important Hg carrier in ice-cores (Jitaru et al., 2009; Vandal et al., 1993), and studies have shown evidence for notable redistribution of terrestrial Hg during the LGM owing to changes in regional atmospheric dust deposition (de Lacerda et al., 2017; Fadina et al., 2019; Pérez-Rodríguez et al., 2015). ~~However, marine sediment records fail to capture measurable changes in dust fluxes over the Ionian and Aegean seas corresponding to MIS 2 (Ehrmann and Schmiedl, 2021). We also see no clear evidence atmospheric dust played a major (direct) role in the local Hg cycle in our data. For example, peaks in elemental ratios typically associated with mineral dust deposits (e.g., Zr/Ti) do not correspond to peaks in $Hg_T$ and/or $Hg_{AR}$ (Vogel et al., 2010), and marine sediment records also fail to capture measurable changes in dust fluxes over the Ionian and Aegean seas corresponding to pronounced Hg signals in Lake Ohrid (Ehrmann and Schmiedl, 2021).~~ However, we see no clear evidence atmospheric dust played a major (direct) role in the local Hg cycle in our data. For example,

peaks in elemental ratios typically associated with mineral dust deposits (e.g., Zr/Ti) do not correspond to peaks in $Hg_T$ and/or $Hg_{AR}$ (**Fig. S7**) (Vogel et al., 2010), nor loess-based evidence for elevated aeolian dust fluxes over Central Europe and the Balkans during the last glacial maximum (Újvári et al., 2010; Rousseau et al., 2021). Marine sediment records also do not capture measurable changes in Saharan dust influx to the Ionian and Aegean seas corresponding to pronounced Hg signals in Lake Ohrid (**Fig. S7**) (Ehrmann and Schmiedl, 2021). Therefore, we cannot mechanistically link elevated Hg values during MIS 2 in Lake Ohrid to broad-scale changes in atmospheric dust deposition.

The largest $Hg_T$ and $Hg_{AR}$ peaks in Lake Prespa occur between 21.3 (±1.7 (1σ from the Bayesian age model, see **Fig. 3**)) ka and 17.5 (±0.7, (1σ)) ka. These signals do not correspond to a measurable change in host phase availability (**Fig. 5**), so it is unlikely that these peaks reflect changes in TOC, TS, and/or K. However, they do coincide with deglaciation of the Pindus and Dinaric mountains (**Fig. 7**) (Hughes et al., 2023). Geomorphological evidence suggests that glaciers were present across the Prespa/Ohrid region between ~26.5 and 15 ka (Belmecheri et al., 2009; Gromig et al., 2018; Ribolini et al., 2018; Ruszkiczay-Rüdiger et al., 2020), and indeed that periglacial processes created a landscape characterized by intense weathering, erosion and sediment transport (Hughes and Woodward, 2017; Allard et al., 2021). Glacial meltwaters thus likely constituted a major source of water input to Lake Prespa during the last deglaciation. Glaciers are important sinks for atmospheric Hg deposited by both dry and wet processes (Durnford and Dastoor, 2011; Zhang et al., 2012), and large quantities of Hg can accumulate in organic-rich frozen soils (permafrost, Schuster et al., 2018). High proportions of detrital matter within glacial ice, snow, and organic matter facilitate the effective, long-term (>100s-1000s of years) retention of atmospheric Hg, meaning that rapid snow/ice melt and permafrost thawing can produce transient 'pulses' of Hg into lakes without a comparable peak in sediment influx (Durnford and Dastoor, 2011; Kohler et al., 2022). This is consistent with the abrupt and short-lived increase in Hg concentration expression of the Hg signal retained in Lake Prespa between 21.3 and 17.5 (±1.7–0.7 (1σ)) ka, which occurs in the absence of a pronounced change in terrigenous elements (e.g., Ti, Rb) or sulphides TS (**Fig. 5, 7**).

Lakes Ohrid and Prespa show two other striking differences in Hg concentration between 35–12 ka (**Fig. 7**). First, Lake Prespa does not record a distinct $Hg_T$ or $Hg_{AR}$ signal during the LGM, and second, Lake Ohrid does not record a distinct $Hg_T$ or $Hg_{AR}$ signal corresponding to deglaciation. Although in Lake Ohrid $Hg_{AR}$ is generally elevated during the LGM and deglaciation, a distinct Hg signal corresponding to deglaciation as recorded in Prespa is not captured (**Fig. 7**). Given their close proximity and environmental similarity, both lakes could be expected to record similar overall signals if the climate-driven processes influencing $Hg_{AR}$ were broadly similar. Given their close proximity and environmental similarity, both lakes could be expected to record similar overall signals if the climate-driven processes influencing $Hg_{AR}$ were broadly similar. One plausible explanation could be a disproportionately large change in Lake Prespa's total volume compared to Lake Ohrid. Increased abundance of small *Fragilariaceae* and benthic *Eolimna submuralis* diatom species point to generally low temperatures and lake levels during MIS 2 (Cvetkoska et al., 2015). These conditions are also

indicated by elevated concentrations of ice-rafted coarse sand and gravel grains, and further suggest persistent ice formation on the lake surface, likely facilitated by the lake's shallow depth (Damaschke et al., 2013; Wagner et al., 2010; Vogel et al., 2010). It is possible that the heightened presence of ice at the peak of glaciation served as a natural barrier between the surface and the sediments of Lake Prespa, effectively slowing the net flux of Hg into delivery of solutes to the basin. A simultaneous lack of ice cover on Lake Ohrid, linked to greater water depths, could also justify why $Hg_{AR}$ remained high in this lake during the LGM, as the Hg influx pathway would be unaffected by ice formation (**Fig. 7**).

Water volume changes may have also influenced the hydrological connection between lakes Ohrid and Prespa during deglaciation ~~Part of the disparity may relate to a change in the lake's hydrological connection to Lake Prespa~~ (Cvetkoska et al., 2016; Jovanovska et al., 2016; Leng et al., 2010). Tracer experiments and stable isotope ($\delta^{18}O$) analysis suggest that water draining from Lake Prespa accounts for a significant proportion of Lake Ohrid's water inflow alongside precipitation (Matzinger et al., 2006; Wagner et al., 2010; Lacey and Jones, 2018), with high rates of prior calcite precipitation occurring in the connecting karst system (Eftimi et al., 1999; Leng et al., 2010; Matzinger et al., 2006). However, ~~decreases in the reconstructed~~a change to lower $\delta^{18}O$ of lakewater and TIC in both lakes during the last glaciation point to a reduction in the contribution of karst-fed waters to Lake Ohrid (Lacey et al., 2016; Leng et al., 2013). Although it is unlikely that the two hydrological systems became completely decoupled (Belmecheri et al., 2009; Lézine et al., 2010), evidence for permafrost formation at high elevations between 35 and 18 ka (Oliva et al., 2018) and lower precipitation ~~(**Fig. 7**)~~ could be linked to a reduction in karst aquifer activity (**Fig. 7**). For shallower Lake Prespa, lower precipitation may also have led to a larger reduction in lake volume compared to Lake Ohrid, decrease in the number (and pressure) of active sinkholes, and subsequently the outflow of water and solutes (e.g., Hg) into Lake Ohrid~~For Lake Prespa, a measurable change in lake volume would reduce the number (and pressure) of active sinkholes (Wagner et al., 2014), and subsequently the outflow of water and solutes (e.g., Hg) into Lake Ohrid~~ (Wagner et al., 2014a) – increasing both $Hg_T$ and $Hg_{AR}$. Together, the collective impact of disproportionately large, climate-driven reductions in water level could explain why rates of Hg accumulation were significantly higher in Lake Prespa during deglaciation compared to the LGM. Glacial meltwaters would elevate the net Hg input compared to the LGM, and reduced ice cover would permit a more direct pathway for Hg to be delivered into the basin; both processes becoming effective while underground permafrost continued to limit the intra-basin exchange of water and solutes.~~We speculate that this may result in higher rates of Hg accumulation in Lake Prespa during intervals of low lake level, where water inputs originated mainly from glacial meltwaters.~~

Neither Lake Ohrid nor Lake Prespa show~~s~~ large changes in Hg concentration nor accumulation ~~large Hg signals~~ during the Oldest (17.5-14.5 ka) and Younger (12.9 – 11.7~~-11.7~~ ka) Dryas. Both lakes contain clear evidence for an abrupt return to glacial conditions during this time. Lake Prespa sediments record shifts in tree pollen and diatom assemblages alluding to a net reduction in local winter temperatures and moisture availability (Aufgebauer et al., 2012a; Panagiotopoulos et al., 2013;

Cvetkoska et al., 2014), and high uranium ($^{234}U/^{238}U$) activity ratios, low tree pollen percentages, and low TIC concentrations in Lake Ohrid also pertain to intense hillslope erosion owing to a more open catchment structure (Francke et al., 2019b; Lézine et al., 2010). Geomorphological evidence also pertains to local glacier stabilization (Gromig et al., 2018; Ribolini et al., 2018; Ruszkiczay-Rüdiger et al., 2020) (**Fig. 7**). Nonetheless, we suggest these events may have been ~~, despite evidence for an abrupt return of glacial conditions (Aufgebauer et al., 2012; Cvetkoska et al., 2015; Panagiotopoulos et al., 2014) and local glacier stabilization (Gromig et al., 2018; Ribolini et al., 2018; Ruszkiczay-Rüdiger et al., 2020) (**Fig. 7**). We posit that these events were either~~ too (a) short-lived, and/or (b) climatically mild to produce ~~the same~~a similarly distinct response in the terrestrial Hg cycle as the processes operating during, and immediately following, the LGM – potentially explaining ~~, which could explain~~ the lack of an associated sedimentary signal.

### 4.3.3. Holocene (12–0 ka; MIS1)

The timing and amplitude of $Hg_T$ and $Hg_{AR}$ signals recorded in Lake Prespa and Lake Ohrid sediments are noticeably different during the Holocene ~~interglacial~~ (MIS 1). Between 12±0.5 and 3±0.2 ka~~~12 and 3 (±0.5–0.2 (1σ)) ka~~, Lake Prespa captures a series of large peaks in $Hg_T$ and $Hg_{AR}$, corresponding to high TOC and TIC indicative of elevated productivity, higher rates of organic material preservation, and limited mixing (**Fig. 5**). ~~whereas~~ Conversely, $Hg_T$ and $Hg_{AR}$ ~~these same proxies~~ show a progressive decline in Lake Ohrid during MIS 1, despite coeval increases in TOC and TIC (**Fig. ~~7~~6**). These observations suggest that for most of the Holocene Hg fluxes into the two lakes were largely decoupled, likely due to differences in catchment and basin dynamics which impacted the rate of Hg delivery to (and burial in) the lakes.

Divergent Hg signals in Lake Ohrid and Lake Prespa during this time may be linked to heightened wildfire frequency and/or intensity. Wildfires have the capacity to (in)directly release Hg from vegetation, and/or through associated changes in soil erosion. Proxy evidence alludes to interglacial conditions characterised by heightened seasonality, characterized by very warm, dry summers coupled with wet, mild winters, an overall increase in the prevalence of deciduous tree species (Cvetkoska et al., 2014; Panagiotopoulos, 2013); but also an increase in macro and microcharcoal concentrations in Lake Prespa (**Fig.7**; Panagiotopoulos et al. 2013). Large wildfires would have a broadly regional-scale impact which, given the close proximity of our two lakes, could theoretically produce a measurable Hg signal in both systems. However, more frequent and/or intense regional fires could also yield measurably different sedimentary Hg signals by their capacity to: (1) enhance surface run off without a corresponding increase in erosion and effectively reduce transport of catchment sourced, mineral-hosted Hg (Mataix-Solera et al., 2011; Shakesby, 2011); (2) enhance downstream transport of Hg released from burned soils and bound to fine and coarse particulate matter (Burke et al., 2010; Takenaka et al., 2021); and/or (3) release large quantities of Hg into the atmosphere following biomass combustion (Howard et al., 2019; Melendez-Perez et al., 2014; Roshan and Biswas, 2023). All three combine to generate impacts that may vary in significance owing to lake-specific differences in sedimentation, accumulation, and flux of materials to/from the lake.

An increase in wildfire activity also corresponds to a period of intensifying human influence in the region; predominantly in the form of land use change, agriculture, and animal husbandry (Cvetkoska et al., 2014; Masi et al., 2018; Panagiotopoulos et al., 2013; Rothacker et al., 2018; Thienemann et al., 2017; Wagner et al., 2009). Widespread mineral resource exploitation and metalworking on the Balkan peninsula is recorded as early as ~8 ka (Gajić-Kvaščev et al., 2012; Longman et al., 2018; Radivojević and Roberts, 2021; Schotsmans et al., 2022), and release of detrital Hg during cinnabar ore extraction and use of Hg in gold extraction (amalgamation) has been linked to pronounced Hg contamination in modern sedimentary units in the region (Covelli et al., 2001; Fitzgerald and Lamborg, 2013). Directly quantifying the influence of (hydro)climate- versus human-driven impacts on sedimentary Hg records presents a major challenge as these factors are interdependent. Nonetheless, these factors could produce a more measurable effect in lake systems with heightened sensitivity to changes in water, nutrient and pollutant fluxes. This could explain why large Hg signals are observed in Lake Prespa between ~12 and 3 ka but not Lake Ohrid: Lake Prespa is shallow relative to its surface area (**Fig. 2**), meaning that relatively small oscillations in pollutant influxes can lead to appreciable changes in lake geochemistry (Cvetkoska et al., 2015; Matzinger et al., 2006).

Decoupling of the two Hg records effectively disappears ~3 ka ago, where both lakes show a sharp and pronounced rise in $Hg_T$ and $Hg_{AR}$ (**Fig. 7**). Several lines of evidence point to human activity as the primary cause. On a local scale, a rapid increase in the biological productivity (eutrophication) of Lake Prespa since ~1.6 (±0.06) ka alludes to greater disturbance of catchment soils by agricultural practices, and eventually use of inorganic compounds such as pesticides and fertilizers (Aufgebauer et al., 2012; Cvetkoska et al., 2014; Krstić et al., 2012; Leng et al., 2013). Signals observed in **Figure 7** may thus be a product of human-induced changes in organic or minerogenic material flux: each facilitating more efficient delivery of catchment-sourced Hg (Fitzgerald et al., 2005), and possibly also stimulating microbial Hg methylation within the sediment (Soerensen et al., 2016). On a broader scale peaks in $Hg_T$ and $Hg_{AR}$ correspond to a sustained rise in European and/or global Hg emissions, owing to increased deforestation, fossil fuel extraction and combustion, and intentional use of Hg for resource extraction/production (Outridge et al., 2018; United Nations Environment Programme, 2018). An increasing number of sedimentary archives record ~~coeval~~ Hg enrichments as early as ~3 ka ago (Biskaborn et al., 2021; Guédron et al., 2019; Li et al., 2020; Pan et al., 2020). The emergence of simultaneous $Hg_T$ and $Hg_{AR}$ peaks in Lakes Ohrid and Prespa following ~3 ka underscores the magnitude and global distribution of this change in Hg sources and emissions (**Fig. 7**), and point to a rise in Hg fluxes between 3 and 0 ka that was distinct enough to effectively overwhelm previously dominant natural drivers of Hg variability.

### 4.4. Key differences & implications

The magnitude and expression of Hg signals recorded in Lake Prespa and Lake Ohrid are different in three aspects. First, the extent to which different host phases can (or cannot) explain time-varying patterns in Hg concentration differs between the two lakes. Although only a limited fraction of Hg

variability in either record can be explained by availability of any single host phase, the low degree of covariance that we do observe points to organic material playing the most significant role as a Hg host in Lake Prespa. In contrast, Hg correlates most strongly with detrital minerals in Lake Ohrid over the same period (0-90 ka) (**Fig. 4**). The second difference is visible during the last glaciation (~35–12 ka): in Lake Ohrid Hg concentrations peak during the LGM (35.8–12 ka), whereas Lake Prespa captures transient, high-amplitude peaks during deglaciation, starting ~15-kyr later (**Fig. 7**). The third difference is visible during the Holocene. The largest signals in the entire Lake Prespa record are observed between ~8 and 0 ka, whereas Hg concentrations do not increase in Lake Ohrid until ~2 ka. These observations raise the question: *for two lakes located in such close geographical proximity and having experienced similar climate conditions, what may have caused such pronounced differences from ~35 ka* (**Fig. 2**)?

Differences in ~~sediment composition, water balance,~~ bathymetric structure~~, and catchment dynamics~~ may ~~all~~ offer a plausible explanation~~s~~. For example, the largest changes in the amplitude and frequency of peaks in $Hg_T$ and $Hg_{AR}$ are exhibited by Lake Prespa (**Fig. 7**): a shallow basin that contains >90 % less water than Lake Ohrid, despite only a ~30 % difference in surface area (Wagner et al., 2010). Increased distance from lake margin to core site in Lake Ohrid would mean distribution of material over a greater total area, and thus more time for net Hg loss to occur either by evasion from the water surface (Cooke et al., 2020), removal of water (and suspended material) via riverine outlets (Bishop et al., 2020), or processes taking place within the water column (Frieling et al., 2023) prior to burial. Therefore, preservation of a measurable Hg signal in a deep lake (e.g., Lake Ohrid) would require notably larger influx of Hg, and this sedimentary signal would also likely be significantly smaller than the equivalent 'dose' delivered to a smaller and/or shallower lake (e.g., Lake Prespa). Coupled with evidence for high-amplitude fluctuations in lake water $\delta^{18}O$ (±6‰) (Leng et al., 2010) and lake level (Cvetkoska et al., 2015, 2016) corresponding to pronounced Hg variability in Lake Prespa, but not in Lake Ohrid (**Fig. 7**), our data suggest that smaller, shallower lakes may be particularly sensitive recorders of transient, changes in Hg fluxes. ~~Materials delivered to a large and/or deep lake (e.g., Lake Ohrid) would be distributed over a greater total area, and must travel notably farther to reach the coring site (Hinderer and Einsele, 2001). This would require a sufficiently large influx of Hg to produce a detectable signal, and is more likely to produce a sedimentary signal that is significantly smaller than the equivalent 'dose' delivered to a smaller and/or shallower lake (e.g., Lake Prespa); even if coring sites are equal distance from the shorelines of their respective basins. Lake Prespa also shows pronounced variability in lake water $\delta^{18}O$ (±6‰) (Leng et al., 2010), frequent lake level fluctuations (Cvetkoska et al., 2015), and slower rates of biological recovery following abrupt disturbance compared to Lake Ohrid (Cvetkoska et al., 2016; Jovanovska et al., 2016), but also the most pronounced changes in the amplitude and frequency of peaks in $Hg_T$ and $Hg_{AR}$ (**Fig. 7**). Thus, shallow lakes are likely more sensitive to changes in erosion, nutrient status, hydrology, and potentially also changes in terrestrial Hg cycling.~~

Divergent bathymetric structures are also linked to distinct differences in biological composition and nutrient availability in lakes Ohrid and Prespa. The deep (~240 m) waters of Lake Ohrid host a highly

oligotrophic (nutrient poor) environment characterized by low levels of biological productivity, and a high abundance of planktonic diatom species (e.g., *Cyclotella*) (Cvetkoska et al., 2021). Conversely, Lake Prespa's shallower (~14 m) waters host a dominantly mesotrophic (nutrient-rich) system in which benthic and planktonic diatom species are present in equal abundance (Jovanovska et al., 2016; Cvetkoska et al., 2016), and allude to moderate/high biological productivity (Leng et al., 2013). Productivity is a potentially important factor influencing the Hg composition of lake sediment: high productivity typically favours higher concentrations of algal biomass, allowing for more effective Hg scavenging by organic particles and export to the sediment (Biester et al., 2018; Soerensen et al., 2016; Hermanns et al., 2013). While the overall signal will remain dominated by Hg availability, broad-scale differences in productivity between lakes Prespa and Ohrid through time could provide an additional explanation for the disparate expression of recorded Hg signals (**section 4.1**); with notably higher productivity in the shallower Lake Prespa further increasing its sensitivity to changes in nutrient status, erosion, and hydrology.

Local differences in Hg emission by neotectonic activity may have also contributed to the divergent Hg signals, owing to differences in the host rock geology, tectonic instability, and mechanical stress regimes of faults surrounding the two basins (Hoffmann et al., 2010; Lindhorst et al., 2015). However, the significance of these differences cannot be fully assessed in the absence of direct Hg emission measurements (see **SD4**).

The two records presented here highlight that Hg cycling in lacustrine environments is distinct from open marine systems. In marine systems, Hg fluxes can be broadly modulated by large-scale continental sediment (Fadina et al., 2019; Figueiredo et al., 2022; Kita et al., 2016) and/or atmospheric inputs (Chede et al., 2022), and Hg burial flux ultimately becomes more closely related to host-phase availability. Conversely, both Lake Prespa and Lake Ohrid highlight how the local basin and catchment characteristics both exert a key control on the delivery of Hg to lacustrine sediments, and suggest that differences in Hg cycling between geographically-proximal basins could occur as a function of diverse physical, hydrological, and biological properties ~~reinforce how smaller, shallower lakes may be particularly sensitive recorders of transient changes in these fluxes~~.

Our observations highlight that multi-millennial lacustrine Hg records allow a different perspective of the Hg cycle compared to marine records, and, for example, may be used to infer how local, regional and global climatic conditions could have altered processes important to the terrestrial Hg cycle. Because lacustrine records are much better suited to recording smaller-scale processes it is also clear that extrapolating the (non-marine) Hg cycle response from a single lacustrine Hg record is challenging. For example, a single-core approach could produce a large degree of uncertainty owing to variable sediment focussing and catchment-sourced influx of organic and inorganic materials (Blais and Kalff, 1995; Engstrom and Rose, 2013; Engstrom and Wright, 1984). A valuable next step would be to apply a source-to-sink approach within a well-known lacustrine catchment and assess the extent to which Hg sedimentation is spatially heterogeneous within a lacustrine system, and whether multiple cores extracted from different locations within the same basin would yield markedly different Hg trends. Intra-basin heterogenetity in Hg sources, reactions, and transformations could also be

examined through measurement of stable Hg isotopes; particularly in millennia-scale sedimentary records where the nature of these processes may change through time (Blum et al., 2014; Jiskra et al., 2022; Kurz et al., 2019). Work of this nature would make great strides toward assessing how representative of variability in the local Hg cycle a single, in this case lake, core is, and whether intra-basin fluctuations in sedimentation, resuspension, and erosion could translate to measurable changes in sedimentary Hg burial.

Past changes in environmental Hg availability inferred from sedimentary records have typically been examined (and presented) by normalizing Hg to a dominant host phase, often taken as organic matter (Fadina et al., 2019; Figueiredo et al., 2020; Grasby et al., 2019; Kita et al., 2016; Percival et al., 2015). However, availability of organic matter or other host phases that scavenge Hg here appear to represent just one of several processes governing Hg burial in lacustrine systems, and this process is very likely systematically less significant compared to marine records in lieu of changes in catchment and basin processes such as erosion, nutrient status, and hydrology (Outridge et al., 2019). Outside pre-industrial times (or periods without an overwhelming global Hg cycle perturbation; such as during LIP formation (Grasby et al., 2019)), a single common process/mechanism is therefore unlikely to produce a unanimous stratigraphic signal across all lakes or even for two adjacent lakes as shown in this study.

## 6. Conclusions

To better understand local and regional impact of climate, vegetation and catchment characteristics on lacustrine Hg records, we present two new high-resolution, Hg records for the last ~90 kyr from Lake Prespa and Lake Ohrid. The two records show some similarities but also distinct differences in the strength of the relationships between Hg, TOC, TS, and detrital minerals (K), with only a relatively small proportion of Hg variability attributable to host phase availability in each record. Our findings provide three valuable insights. First, that local sedimentary environment does influence Hg burial. Covariance with host phases accounts for a limited proportion of the observed variability, suggesting that many of the $Hg_T$ and $Hg_{AR}$ signals recorded in Lake Prespa and Lake Ohrid reflect net Hg input to the two lakes across timescales ranging from decades to multiple millennia. Second, Hg signals can reflect changes in (and also differences between) ~~changes (and also differences)~~ in catchment hydrology and structure. Despite their proximity, the magnitude and expression of the recorded signals are considerably different between Lake Prespa and Lake Ohrid, suggesting these inputs changed relative to sedimentary setting and in response to changing interactions between the two systems. Finally, regional-scale climate variability can measurably affect the Hg signals retained in lake sediments: both lakes Prespa and Ohrid showing changes in Hg concentration and accumulation corresponding to glacial (late Pleistocene) and interglacial (Holocene) climate conditions. It follows that local, regional, or global changes in climate or hydrological cycling capable of affecting mineral soils, (peri-)glacial features or fire regime in the lake catchment could all impact Hg fluxes. These findings prompt further examination of how orbital-scale climate variability (>$10^3$-year timescales) may

influence the terrestrial Hg cycle, not only to better resolve processes acting on single lacustrine and terrestrial successions, but also to identify which of these (local) processes could hold relevance for Hg cycling on a global scale.

## Competing Interests

The corresponding author declares that none of the authors have any competing interests.

## Acknowledgements

ARP, IMF, JF, and TAM acknowledge funding from European Research Council Consolidator Grant V-ECHO (ERC-2018-COG-818717-V-ECHO). ARP thanks Professor David Thomas and Mona Edwards (School of Geography, Oxford) for logistical assistance with sample transfer and storage. KP acknowledges funding from the German Research Foundation (DFG grant PA 2664/4-1). All authors thank members of the Scientific Collaboration on Past Speciation Conditions in Lake Ohrid (SCOPSCO), and the CRC 806 "*Our Way to Europe - Culture-Environment Interaction and Human Mobility in the Late Quaternary*" projects: for their efforts in producing the Lake Ohrid and Lake Prespa sediment successions, and making the data available for scientific use.

## References Cited

Allard, J. L., Hughes, P. D., Woodward, J. C., Fink, D., Simon, K., and Wilcken, K. M.: Late Pleistocene glaciers in Greece: A new 36Cl chronology, Quaternary Science Reviews, 245, 106528, https://doi.org/10.1016/j.quascirev.2020.106528, 2020.

Allard, J. L., Hughes, P. D., and Woodward, J. C.: A radiometric dating revolution and the Quaternary glacial history of the Mediterranean mountains, Earth-Science Reviews, 223, 103844, https://doi.org/10.1016/j.earscirev.2021.103844, 2021.

Aufgebauer, A., Panagiotopoulos, K., Wagner, B., Schaebitz, F., Viehberg, F. A., Vogel, H., Zanchetta, G., Sulpizio, R., Leng, M. J., and Damaschke, M.: Climate and environmental change in the Balkans over the last 17 ka recorded in sediments from Lake Prespa (Albania/F.Y.R. of Macedonia/Greece), Quaternary International, 274, 122–135, https://doi.org/10.1016/j.quaint.2012.02.015, 2012.

Belmecheri, S., Namiotko, T., Robert, C., von Grafenstein, U., and Danielopol, D. L.: Climate controlled ostracod preservation in Lake Ohrid (Albania, Macedonia), Palaeogeography, Palaeoclimatology, Palaeoecology, 277, 236–245, https://doi.org/10.1016/j.palaeo.2009.04.013, 2009.

Benoit, J. M., Gilmour, C. C., Mason, R. P., and Heyes, A.: Sulfide controls on mercury speciation and bioavailability to methylating bacteria in sediment pore waterA, Environmental Science and Technology, 33, 1780, https://doi.org/10.1021/es992007q, 1999.

Biester, H., Pérez-Rodríguez, M., Gilfedder, B.-S., Martínez Cortizas, A., and Hermanns, Y.-M.: Solar irradiance and primary productivity controlled mercury accumulation in sediments of a remote lake in the Southern Hemisphere during the past 4000 years: Primary productivity and mercury accumulation, Limnol. Oceanogr., 63, 540–549, https://doi.org/10.1002/lno.10647, 2018.

Bin, C., Xiaoru, W., and Lee, F. S. C.: Pyrolysis coupled with atomic absorption spectrometry for the determination of mercury in Chinese medicinal materials, Analytica Chimica Acta, 447, 161–169, https://doi.org/10.1016/S0003-2670(01)01218-1, 2001.

Bini, M., Zanchetta, G., Perşoiu, A., Cartier, R., Català, A., Cacho, I., Dean, J. R., Di Rita, F., Drysdale, R. N., Finnè, M., Isola, I., Jalali, B., Lirer, F., Magri, D., Masi, A., Marks, L., Mercuri, A. M., Peyron, O., Sadori, L., Sicre, M. A., Welc, F., Zielhofer, C., and Brisset, E.: The 4.2 ka BP Event in the Mediterranean region: An overview, Climate of the Past, 15, 555–577, https://doi.org/10.5194/cp-15-555-2019, 2019.

Bishop, K., Shanley, J. B., Riscassi, A., de Wit, H. A., Eklöf, K., Meng, B., Mitchell, C., Osterwalder, S., Schuster, P. F., Webster, J., and Zhu, W.: Recent advances in understanding and measurement of mercury in the environment: Terrestrial Hg cycling, Science of the Total Environment, 721, https://doi.org/10.1016/j.scitotenv.2020.137647, 2020.

Biskaborn, B. K., Narancic, B., Stoof-Leichsenring, K. R., Pestryakova, L. A., Appleby, P. G., Piliposian, G. T., and Diekmann, B.: Effects of climate change and industrialization on Lake Bolshoe Toko, eastern Siberia, J Paleolimnol, 65, 335–352, https://doi.org/10.1007/s10933-021-00175-z, 2021.

Blaauw, M. and Christeny, J. A.: Flexible paleoclimate age-depth models using an autoregressive gamma process, Bayesian Analysis, 6, 457–474, https://doi.org/10.1214/11-BA618, 2011.

Blais, J. M. and Kalff, J.: The influence of lake morphometry on sediment focusing, Limnol. Oceanogr., 40, 582–588, https://doi.org/10.4319/lo.1995.40.3.0582, 1995.

Blum, J. D., Sherman, L. S., and Johnson, M. W.: Mercury Isotopes in Earth and Environmental Sciences, Annu. Rev. Earth Planet. Sci., 42, 249–269, https://doi.org/10.1146/annurev-earth-050212-124107, 2014.

Branfireun, B. A., Cosio, C., Poulain, A. J., Riise, G., and Bravo, A. G.: Mercury cycling in freshwater systems - An updated conceptual model, Science of the Total Environment, 745, https://doi.org/10.1016/j.scitotenv.2020.140906, 2020.

Burke, M. P., Hogue, T. S., Ferreira, M., Mendez, C. B., Navarro, B., Lopez, S., and Jay, J. A.: The Effect of Wildfire on Soil Mercury Concentrations in Southern California Watersheds, Water Air Soil Pollut, 212, 369–385, https://doi.org/10.1007/s11270-010-0351-y, 2010.

Carrivick, J. L. and Tweed, F. S.: Deglaciation controls on sediment yield: Towards capturing spatio-temporal variability, Earth-Science Reviews, 221, 103809, https://doi.org/10.1016/j.earscirev.2021.103809, 2021.

Chakraborty, P., Sarkar, A., Vudamala, K., Naik, R., and Nath, B. N.: Organic matter - A key factor in controlling mercury distribution in estuarine sediment, Marine Chemistry, 173, 302–309, https://doi.org/10.1016/j.marchem.2014.10.005, 2015.

Chede, B. S., Venancio, I. M., Figueiredo, T. S., Albuquerque, A. L. S., and Silva-Filho, E. V.: Mercury deposition in the western tropical South Atlantic during the last 70 ka, Palaeogeography, Palaeoclimatology, Palaeoecology, 601, 111122, https://doi.org/10.1016/j.palaeo.2022.111122, 2022.

Cooke, C. A., Martínez-Cortizas, A., Bindler, R., and Sexauer Gustin, M.: Environmental archives of atmospheric Hg deposition – A review, Science of the Total Environment, 709, 134800, https://doi.org/10.1016/j.scitotenv.2019.134800, 2020.

Cordeiro, R. C., Turcq, B., Sifeddine, A., Lacerda, L. D., Silva Filho, E. V., Gueiros, B., Potty, Y. P., Santelli, R. E., Pádua, E. O., and Patchineiam, S. R.: Biogeochemical indicators of environmental changes from 50Ka to 10Ka in a humid region of the Brazilian Amazon, Palaeogeography, Palaeoclimatology, Palaeoecology, 299, 426–436, https://doi.org/10.1016/j.palaeo.2010.11.021, 2011.

Covelli, S., Faganeli, J., Horvat, M., and Brambati, A.: Mercury contamination of coastal sediments as the result of long-term cinnabar mining activity (Gulf of Trieste, northern Adriatic sea), Applied Geochemistry, 16, 541–558, https://doi.org/10.1016/S0883-2927(00)00042-1, 2001.

Cvetkoska, A., Levkov, Z., Reed, J. M., and Wagner, B.: Late Glacial to Holocene climate change and human impact in the Mediterranean: The last ca. 17ka diatom record of Lake Prespa (Macedonia/Albania/Greece), Palaeogeography, Palaeoclimatology, Palaeoecology, 406, 22–32, https://doi.org/10.1016/j.palaeo.2014.04.010, 2014.

Cvetkoska, A., Levkov, Z., Reed, J. M., Wagner, B., Panagiotopoulos, K., Leng, M. J., and Lacey, J. H.: Quaternary climate change and Heinrich events in the southern Balkans: Lake Prespa diatom palaeolimnology from the last interglacial to present, Journal of Paleolimnology, 53, 215–231, https://doi.org/10.1007/s10933-014-9821-3, 2015.

Cvetkoska, A., Jovanovska, E., Francke, A., Tofilovska, S., Vogel, H., Levkov, Z., Donders, T. H., Wagner, B., and Wagner-Cremer, F.: Ecosystem regimes and responses in a coupled ancient lake system from MIS 5b to present: the diatom record of lakes Ohrid and Prespa, Biogeosciences, 13, 3147–3162, https://doi.org/10.5194/bg-13-3147-2016, 2016.

Cvetkoska, A., Jovanovska, E., Hauffe, T., Donders, T. H., Levkov, Z., Van De Waal, D. B., Reed, J. M., Francke, A., Vogel, H., Wilke, T., Wagner, B., and Wagner-Cremer, F.: Drivers of phytoplankton community structure change with ecosystem ontogeny during the Quaternary, Quaternary Science Reviews, 265, 107046, https://doi.org/10.1016/j.quascirev.2021.107046, 2021.

Damaschke, M., Sulpizio, R., Zanchetta, G., Wagner, B., Böhm, A., Nowaczyk, N., Rethemeyer, J., and Hilgers, A.: Tephrostratigraphic studies on a sediment core from Lake Prespa in the Balkans, Climate of the Past, 9, 267–287, https://doi.org/10.5194/cp-9-267-2013, 2013.

Ding, X., Li, D., Zheng, L., Bao, H., Chen, H.-F., and Kao, S.-J.: Sulfur Geochemistry of a Lacustrine Record from Taiwan Reveals Enhanced Marine Aerosol Input during the Early Holocene, Sci Rep, 6, 38989, https://doi.org/10.1038/srep38989, 2016.

Donders, T., Panagiotopoulos, K., Koutsodendris, A., Bertini, A., Mercuri, A. M., Masi, A., Combourieu-Nebout, N., Joannin, S., Kouli, K., Kousis, I., Peyron, O., Torri, P., Florenzano, A., Francke, A., Wagner, B., and Sadori, L.: 1.36 million years of Mediterranean forest refugium dynamics in response to glacial-interglacial cycle strength, Proceedings of the National Academy of Sciences of the United States of America, 118, https://doi.org/10.1073/pnas.2026111118, 2021.

Driscoll, C. T., Mason, R. P., Chan, H. M., Jacob, D. J., and Pirrone, N.: Mercury as a global pollutant: Sources, pathways, and effects, Environmental Science and Technology, 47, 4967–4983, https://doi.org/10.1021/es305071v, 2013.

Durnford, D. and Dastoor, A.: The behavior of mercury in the cryosphere: A review of what we know from observations, Journal of Geophysical Research Atmospheres, 116, https://doi.org/10.1029/2010JD014809, 2011.

Edwards, B. A., Kushner, D. S., Outridge, P. M., and Wang, F.: Fifty years of volcanic mercury emission research: Knowledge gaps and future directions, Science of the Total Environment, 757, 143800, https://doi.org/10.1016/j.scitotenv.2020.143800, 2021.

Eftimi, R., Skende, P., and Zoto, J.: An isotope study of the connection of Ohrid and Prespa lakes, Geologica Balcanica, 32, 43–49, 1999.

Ehrmann, W. and Schmiedl, G.: Nature and dynamics of North African humid and dry periods during the last 200,000 years documented in the clay fraction of eastern mediterranean deep-sea sediments, Quaternary Science Reviews, 260, 106925, https://doi.org/10.1016/j.quascirev.2021.106925, 2021.

Engstrom, D. R. and Rose, N. L.: A whole-basin, mass-balance approach to paleolimnology, J Paleolimnol, 49, 333–347, https://doi.org/10.1007/s10933-012-9675-5, 2013.

Engstrom, D. R. and Wright, H. E.: Chemical stratigraphy of lake sediments as a record of environmental change, in: Lake Sediments and Environmental History, University of Minnesota Press, 11–67, 1984.

Fadina, O. A., Venancio, I. M., Belem, A., Silveira, C. S., Bertagnolli, D. de C., Silva-Filho, E. V., and Albuquerque, A. L. S.: Paleoclimatic controls on mercury deposition in northeast Brazil since the Last Interglacial, Quaternary Science Reviews, 221, 105869, https://doi.org/10.1016/j.quascirev.2019.105869, 2019.

Figueiredo, T. S., Santos, T. P., Costa, K. B., Toledo, F., Albuquerque, A. L. S., Smoak, J. M., Bergquist, B. A., and Silva-Filho, E. V.: Effect of deep Southwestern Subtropical Atlantic Ocean circulation on the biogeochemistry of mercury during the last two glacial/interglacial cycles, Quaternary Science Reviews, 239, 106368, https://doi.org/10.1016/j.quascirev.2020.106368, 2020.

Figueiredo, T. S., Bergquist, B. A., Santos, T. P., Albuquerque, A. L. S., and Silva-Filho, E. V.: Relationship between glacial CO2 drawdown and mercury cycling in the western South Atlantic: An isotopic insight, Geology, 50, 3–7, https://doi.org/10.1130/g49942.1, 2022.

Fitzgerald, W. F. and Lamborg, C. H.: Geochemistry of Mercury in the Environment, Elsevier Ltd., 91–129 pp., https://doi.org/10.1016/B978-0-08-095975-7.00904-9, 2013.

Fitzgerald, W. F., Engstrom, D. R., Lamborg, C. H., Tseng, C.-M., Balcom, P. H., and Hammerschmidt, C. R.: Modern and Historic Atmospheric Mercury Fluxes in Northern Alaska: Global Sources and Arctic Depletion, Environ. Sci. Technol., 39, 557–568, https://doi.org/10.1021/es049128x, 2005.

Francke, A., Wagner, B., Just, J., Leicher, N., Gromig, R., Baumgarten, H., Vogel, H., Lacey, J. H., Sadori, L., Wonik, T., Leng, M. J., Zanchetta, G., Sulpizio, R., and Giaccio, B.: Sedimentological processes and environmental variability at Lake Ohrid (Macedonia, Albania) between 637 ka and the present, Biogeosciences, 13, 1179–1196, https://doi.org/10.5194/bg-13-1179-2016, 2016.

Francke, A., Dosseto, A., Panagiotopoulos, K., Leicher, N., Lacey, J. H., Kyrikou, S., Wagner, B., Zanchetta, G., Kouli, K., and Leng, M. J.: Sediment residence time reveals Holocene shift from climatic to vegetation control on catchment erosion in the Balkans, Global and Planetary Change, 177, 186–200, https://doi.org/10.1016/j.gloplacha.2019.04.005, 2019.

Frieling, J., Mather, T. A., März, C., Jenkyns, H. C., Hennekam, R., Reichart, G.-J., Slomp, C. P., and Van Helmond, N. A. G. M.: Effects of redox variability and early diagenesis on marine sedimentary Hg records, Geochimica et Cosmochimica Acta, S0016703723001850, https://doi.org/10.1016/j.gca.2023.04.015, 2023.

1007 Gajić-Kvaščev, M., Stojanović, M. M., Šmit, Ž., Kantarelou, V., Karydas, A. G., Šljivar, D., Milovanović, D., and Andrić, V.: New
1008 evidence for the use of cinnabar as a colouring pigment in the Vinča culture, Journal of Archaeological Science, 39, 1025–
1009 1033, https://doi.org/10.1016/j.jas.2011.11.023, 2012.

1010 Garcia-Ordiales, E., Covelli, S., Rico, J. M., Roqueñí, N., Fontolan, G., Flor-Blanco, G., Cienfuegos, P., and Loredo, J.:
1011 Occurrence and speciation of arsenic and mercury in estuarine sediments affected by mining activities (Asturias, northern
1012 Spain), Chemosphere, 198, 281–289, https://doi.org/10.1016/j.chemosphere.2018.01.146, 2018.

1013 Gelety, V. F., Kalmykov, G. V., and Parkhomenko, I. Y.: Mercury in the sedimentary deposits of Lake Baikal, Geochemistry
1014 International, 45, 170–177, https://doi.org/10.1134/S001670290702005X, 2007.

1015 Giaccio, B., Hajdas, I., Isaia, R., Deino, A., and Nomade, S.: High-precision 14C and 40Ar/39 Ar dating of the Campanian
1016 Ignimbrite (Y-5) reconciles the time-scales of climatic-cultural processes at 40 ka, Scientific Reports, 7, 1–10,
1017 https://doi.org/10.1038/srep45940, 2017.

1018 Goosse, H., Brovkin, V., Fichefet, T., Haarsma, R., Huybrechts, P., Jongma, J., Mouchet, A., Selten, F., Barriat, P. Y., Campin,
1019 J. M., Deleersnijder, E., Driesschaert, E., Goelzer, H., Janssens, I., Loutre, M. F., Morales Maqueda, M. A., Opsteegh, T.,
1020 Mathieu, P. P., Munhoven, G., Pettersson, E. J., Renssen, H., Roche, D. M., Schaeffer, M., Tartinville, B., Timmermann, A.,
1021 and Weber, S. L.: Description of the Earth system model of intermediate complexity LOVECLIM version 1.2, Geoscientific
1022 Model Development, 3, 603–633, https://doi.org/10.5194/gmd-3-603-2010, 2010.

1023 Grasby, S. E., Them, T. R., Chen, Z., Yin, R., and Ardakani, O. H.: Mercury as a proxy for volcanic emissions in the geologic
1024 record, Earth-Science Reviews, 196, 102880, https://doi.org/10.1016/j.earscirev.2019.102880, 2019.

1025 Gromig, R., Mechernich, S., Ribolini, A., Wagner, B., Zanchetta, G., Isola, I., Bini, M., and Dunai, T. J.: Evidence for a Younger
1026 Dryas deglaciation in the Galicica Mountains (FYROM) from cosmogenic 36Cl, Quaternary International, 464, 352–363,
1027 https://doi.org/10.1016/j.quaint.2017.07.013, 2018.

1028 Grygar, T. M., Mach, K., and Martinez, M.: Checklist for the use of potassium concentrations in siliciclastic sediments as
1029 paleoenvironmental archives, Sedimentary Geology, 382, 75–84, https://doi.org/10.1016/j.sedgeo.2019.01.010, 2019.

1030 Guédron, S., Tolu, J., Brisset, E., Sabatier, P., Perrot, V., Bouchet, S., Develle, A. L., Bindler, R., Cossa, D., Fritz, S. C., and
1031 Baker, P. A.: Late Holocene volcanic and anthropogenic mercury deposition in the western Central Andes (Lake Chungará
1032 Chile), Science of the Total Environment, 662, 903–914, https://doi.org/10.1016/j.scitotenv.2019.01.294, 2019.

1033 Han, S., Obraztsova, A., Pretto, P., Deheyn, D. D., Gieskes, J., and Tebo, B. M.: Sulfide and iron control on mercury speciation
1034 in anoxic estuarine sediment slurries, Marine Chemistry, 111, 214–220, https://doi.org/10.1016/j.marchem.2008.05.002, 2008.

1035 Hermanns, Y. M., Cortizas, A. M., Arz, H., Stein, R., and Biester, H.: Untangling the influence of in-lake productivity and
1036 terrestrial organic matter flux on 4,250 years of mercury accumulation in Lake Hambre, Southern Chile, Journal of
1037 Paleolimnology, 49, 563–573, https://doi.org/10.1007/s10933-012-9657-7, 2013.

1038 Hoffmann, N., Reicherter, K., Fernández-Steeger, T., and Grützner, C.: Evolution of ancient Lake Ohrid: a tectonic perspective,
1039 Biogeosciences, 7, 3377–3386, https://doi.org/10.5194/bg-7-3377-2010, 2010.

1040 Hollis, G. E. and Stevenson, A. C.: The physical basis of the Lake Mikri Prespa systems: Geology, climate, hydrology and water
1041 quality, Hydrobiologia, 351, 1–19, https://doi.org/10.1023/A:1003067115862, 1997.

1042 Holmer, M. and Storkholm, P.: Sulphate reduction and sulphur cycling in lake sediments: a review: Sulphate cycling in lake
1043 sediments, Freshwater Biology, 46, 431–451, https://doi.org/10.1046/j.1365-2427.2001.00687.x, 2001.

1044 Howard, D., Macsween, K., Edwards, G. C., Desservettaz, M., Guérette, E. A., Paton-Walsh, C., Surawski, N. C., Sullivan, A.
1045 L., Weston, C., Volkova, L., Powell, J., Keywood, M. D., Reisen, F., and (Mick) Meyer, C. P.: Investigation of mercury emissions
1046 from burning of Australian eucalypt forest surface fuels using a combustion wind tunnel and field observations, Atmospheric
1047 Environment, 202, 17–27, https://doi.org/10.1016/j.atmosenv.2018.12.015, 2019.

1048 Hughes, P. D. and Woodward, J. C.: Quaternary glaciation in the Mediterranean mountains: A new synthesis, Geological
1049 Society Special Publication, 433, 1–23, https://doi.org/10.1144/SP433.14, 2017.

1050 Hughes, P. D., Woodward, J. C., Gibbard, P. L., Macklin, M. G., Gilmour, M. A., and Smith, G. R.: The glacial history of the
1051 Pindus Mountains, Greece, Journal of Geology, 114, 413–434, https://doi.org/10.1086/504177, 2006.

1052 Hughes, P. D., Allard, J. L., and Woodward, J. C.: The Balkans: glacial landforms prior to the Last Glacial Maximum, European
1053 Glacial Landscapes, 323–332, https://doi.org/10.1016/b978-0-12-823498-3.00034-0, 2022.

1054 Hughes, P. D., Allard, J. L., Woodward, J. C., and Pope, R. J. J.: The Balkans: glacial landforms during deglaciation, in:
1055 European Glacial Landscapes, Elsevier, 221–231, https://doi.org/10.1016/B978-0-323-91899-2.00055-3, 2023.

Jiskra, M., Guédron, S., Tolu, J., Fritz, S. C., Baker, P. A., and Sonke, J. E.: Climatic Controls on a Holocene Mercury Stable Isotope Sediment Record of Lake Titicaca, ACS Earth and Space Chemistry, 6, 346–357, https://doi.org/10.1021/acsearthspacechem.1c00304, 2022.

Jitaru, P., Gabrielli, P., Marteel, A., Plane, J. M. C., Planchon, F. A. M., Gauchard, P. A., Ferrari, C. P., Boutron, C. F., Adams, F. C., Hong, S., Cescon, P., and Barbante, C.: Atmospheric depletion of mercury over Antarctica during glacial periods, Nature Geoscience, 2, 505–508, https://doi.org/10.1038/ngeo549, 2009.

Jovanovska, E., Cvetkoska, A., Hauffe, T., Levkov, Z., Wagner, B., Sulpizio, R., Francke, A., Albrecht, C., and Wilke, T.: Differential resilience of ancient sister lakes Ohrid and Prespa to environmental disturbances during the Late Pleistocene, Biogeosciences, 13, 1149–1161, https://doi.org/10.5194/bg-13-1149-2016, 2016.

Just, J., Nowaczyk, N., Francke, A., Sagnotti, L., and Wagner, B.: Climatic control on the occurrence of high-coercivity magnetic minerals and preservation of greigite in a 640 ka sediment sequence from Lake Ohrid (Balkans), Biogeosciences Discussions, 12, 14215–14243, https://doi.org/10.5194/bgd-12-14215-2015, 2015.

Kita, I., Yamashita, T., Chiyonobu, S., Hasegawa, H., Sato, T., and Kuwahara, Y.: Mercury content in Atlantic sediments as a new indicator of the enlargement and reduction of Northern Hemisphere ice sheets, Journal of Quaternary Science, 31, 167–177, https://doi.org/10.1002/jqs.2854, 2016.

Kohler, S. G., Petrova, M. V, Digernes, M. G., Sanchez, N., Dufour, A., Simić, A., Ndungu, K., and Ardelan, M. V: Arctic Ocean's wintertime mercury concentrations limited by seasonal loss on the shelf, Nature Geoscience, https://doi.org/10.1038/s41561-022-00986-3, 2022.

Kongchum, M., Hudnall, W. H., and Delaune, R. D.: Relationship between sediment clay minerals and total mercury, Journal of Environmental Science and Health - Part A Toxic/Hazardous Substances and Environmental Engineering, 46, 534–539, https://doi.org/10.1080/10934529.2011.551745, 2011.

Krstić, S., Zdraveski, N., and Blinkova, M.: Implementing the WFD in River Basin Management Plans – A Case Study of Prespa Lake Watershed, in: BALWOIS, 2012.

Kurz, A. Y., Blum, J. D., Washburn, S. J., and Baskaran, M.: Changes in the mercury isotopic composition of sediments from a remote alpine lake in Wyoming, USA, Science of the Total Environment, 669, 973–982, https://doi.org/10.1016/j.scitotenv.2019.03.165, 2019.

de Lacerda, L. D., Turcq, B., Sifeddine, A., and Cordeiro, R. C.: Mercury accumulation rates in Caço Lake, NE Brazil during the past 20.000 years, Journal of South American Earth Sciences, 77, 42–50, https://doi.org/10.1016/j.jsames.2017.04.008, 2017.

Lacey, J. H. and Jones, M. D.: Quantitative reconstruction of early Holocene and last glacial climate on the Balkan Peninsula using coupled hydrological and isotope mass balance modelling, Quaternary Science Reviews, 202, 109–121, https://doi.org/10.1016/j.quascirev.2018.09.007, 2018.

Lacey, J. H., Leng, M. J., Francke, A., Sloane, H. H., Milodowski, A., Vogel, H., Baumgarten, H., Zanchetta, G., and Wagner, B.: Northern Mediterranean climate since the Middle Pleistocene: A 637 ka stable isotope record from Lake Ohrid (Albania/Macedonia), Biogeosciences, 13, 1801–1820, https://doi.org/10.5194/bg-13-1801-2016, 2016.

Leicher, N., Giaccio, B., Zanchetta, G., Sulpizio, R., Albert, P. G., Tomlinson, E. L., Lagos, M., Francke, A., and Wagner, B.: Lake Ohrid's tephrochronological dataset reveals 1.36 Ma of Mediterranean explosive volcanic activity, Scientific Data, 8, 1–14, https://doi.org/10.1038/s41597-021-01013-7, 2021.

Leng, M. J., Baneschi, I., Zanchetta, G., Jex, C. N., Wagner, B., and Vogel, H.: Late Quaternary palaeoenvironmental reconstruction from Lakes Ohrid and Prespa (Macedonia/Albania border) using stable isotopes, Biogeosciences, 7, 3109–3122, https://doi.org/10.5194/bg-7-3109-2010, 2010.

Leng, M. J., Wagner, B., Boehm, A., Panagiotopoulos, K., Vane, C. H., Snelling, A., Haidon, C., Woodley, E., Vogel, H., Zanchetta, G., and Baneschi, I.: Understanding past climatic and hydrological variability in the mediterranean from Lake Prespa sediment isotope and geochemical record over the last glacial cycle, Quaternary Science Reviews, 66, 123–136, https://doi.org/10.1016/j.quascirev.2012.07.015, 2013.

Leontaritis, A. D., Kouli, K., and Pavlopoulos, K.: The glacial history of Greece: a comprehensive review, Mediterranean Geoscience Reviews, 2, 65–90, https://doi.org/10.1007/s42990-020-00021-w, 2020.

Lewin, J., Macklin, M. G., and Woodward, J. C.: Late quaternary fluvial sedimentation in the voidomatis basin, Epirus, Northwest Greece, Quaternary Research, 35, 103–115, https://doi.org/10.1016/0033-5894(91)90098-P, 1991.

Lézine, A. M., von Grafenstein, U., Andersen, N., Belmecheri, S., Bordon, A., Caron, B., Cazet, J. P., Erlenkeuser, H., Fouache, E., Grenier, C., Huntsman-Mapila, P., Hureau-Mazaudier, D., Manelli, D., Mazaud, A., Robert, C., Sulpizio, R., Tiercelin, J. J., Zanchetta, G., and Zeqollari, Z.: Lake Ohrid, Albania, provides an exceptional multi-proxy record of environmental changes during the last glacial-interglacial cycle, Palaeogeography, Palaeoclimatology, Palaeoecology, 287, 116–127, https://doi.org/10.1016/j.palaeo.2010.01.016, 2010.

Li, C., Enrico, M., Magand, O., Araujo, B. F., Le Roux, G., Osterwalder, S., Dommergue, A., Bertrand, Y., Brioude, J., De Vleeschouwer, F., and Sonke, J. E.: A peat core Hg stable isotope reconstruction of Holocene atmospheric Hg deposition at Amsterdam Island (37.8oS), Geochimica et Cosmochimica Acta, 341, 62–74, https://doi.org/10.1016/j.gca.2022.11.024, 2023.

Li, F., Ma, C., and Zhang, P.: Mercury Deposition, Climate Change and Anthropogenic Activities: A Review, Frontiers in Earth Science, 8, https://doi.org/10.3389/feart.2020.00316, 2020.

Lindhorst, K., Krastel, S., Reicherter, K., Stipp, M., Wagner, B., and Schwenk, T.: Sedimentary and tectonic evolution of Lake Ohrid (Macedonia/Albania), Basin Res, 27, 84–101, https://doi.org/10.1111/bre.12063, 2015.

Lisiecki, L. E. and Raymo, M. E.: A Pliocene-Pleistocene stack of 57 globally distributed benthic δ 18O records, Paleoceanography, 20, 1–17, https://doi.org/10.1029/2004PA001071, 2005.

Longman, J., Veres, D., Finsinger, W., and Ersek, V.: Exceptionally high levels of lead pollution in the Balkans from the Early Bronze Age to the Industrial Revolution, Proc. Natl. Acad. Sci. U.S.A., 115, https://doi.org/10.1073/pnas.1721546115, 2018.

Lyman, S. N., Cheng, I., Gratz, L. E., Weiss-Penzias, P., and Zhang, L.: An updated review of atmospheric mercury, Science of the Total Environment, 707, 135575, https://doi.org/10.1016/j.scitotenv.2019.135575, 2020.

Masi, A., Francke, A., Pepe, C., Thienemann, M., Wagner, B., and Sadori, L.: Vegetation history and paleoclimate at Lake Dojran (FYROM/Greece) during the Late Glacial and Holocene, Clim. Past, 14, 351–367, https://doi.org/10.5194/cp-14-351-2018, 2018.

Mataix-Solera, J., Cerdà, A., Arcenegui, V., Jordán, A., and Zavala, L. M.: Fire effects on soil aggregation: A review, Earth-Science Reviews, 109, 44–60, https://doi.org/10.1016/j.earscirev.2011.08.002, 2011.

Matzinger, A., Jordanoski, M., Veljanoska-Sarafiloska, E., Sturm, M., Müller, B., and Wüest, A.: Is Lake Prespa jeopardizing the ecosystem of ancient Lake Ohrid?, Hydrobiologia, 553, 89–109, https://doi.org/10.1007/s10750-005-6427-9, 2006.

Melendez-Perez, J. J., Fostier, A. H., Carvalho, J. A., Windmöller, C. C., Santos, J. C., and Carpi, A.: Soil and biomass mercury emissions during a prescribed fire in the Amazonian rain forest, Atmospheric Environment, 96, 415–422, https://doi.org/10.1016/j.atmosenv.2014.06.032, 2014.

Nasr, M., Ogilvie, J., Castonguay, M., Rencz, A., and Arp, P. A.: Total Hg concentrations in stream and lake sediments: Discerning geospatial patterns and controls across Canada, Applied Geochemistry, 26, 1818–1831, https://doi.org/10.1016/j.apgeochem.2011.06.006, 2011.

Obrist, D., Kirk, J. L., Zhang, L., Sunderland, E. M., Jiskra, M., and Selin, N. E.: A review of global environmental mercury processes in response to human and natural perturbations: Changes of emissions, climate, and land use, Ambio, 47, 116–140, https://doi.org/10.1007/s13280-017-1004-9, 2018.

Oliva, M., Žebre, M., Guglielmin, M., Hughes, P. D., Çiner, A., Vieira, G., Bodin, X., Andrés, N., Colucci, R. R., García-Hernández, C., Mora, C., Nofre, J., Palacios, D., Pérez-Alberti, A., Ribolini, A., Ruiz-Fernández, J., Sarıkaya, M. A., Serrano, E., Urdea, P., Valcárcel, M., Woodward, J. C., and Yıldırım, C.: Permafrost conditions in the Mediterranean region since the Last Glaciation, Earth-Science Reviews, 185, 397–436, https://doi.org/10.1016/j.earscirev.2018.06.018, 2018.

Outridge, Sanei, H., Stern, Hamilton, and Goodarzi, F.: Evidence for Control of Mercury Accumulation Rates in Canadian High Arctic Lake Sediments by Variations of Aquatic Primary Productivity, Environ. Sci. Technol., 41, 5259–5265, https://doi.org/10.1021/es070408x, 2007.

Outridge, P. M., Mason, R. P., Wang, F., Guerrero, S., and Heimbürger-Boavida, L. E.: Updated Global and Oceanic Mercury Budgets for the United Nations Global Mercury Assessment 2018, Environmental Science and Technology, 52, 11466–11477, https://doi.org/10.1021/acs.est.8b01246, 2018.

Outridge, P. M., Stern, G. A., Hamilton, P. B., and Sanei, H.: Algal scavenging of mercury in preindustrial Arctic lakes, Limnol Oceanogr, 64, 1558–1571, https://doi.org/10.1002/lno.11135, 2019.

Overeem, I., Hudson, B. D., Syvitski, J. P. M., Mikkelsen, A. B., Hasholt, B., Van Den Broeke, M. R., Noel, B. P. Y., and Morlighem, M.: Substantial export of suspended sediment to the global oceans from glacial erosion in Greenland, Nature Geoscience, 10, 859–863, https://doi.org/10.1038/NGEO3046, 2017.

Pan, J., Zhong, W., Wei, Z., Ouyang, J., Shang, S., Ye, S., Chen, Y., Xue, J., and Tang, X.: A 15,400-year record of natural and anthropogenic input of mercury (Hg) in a sub-alpine lacustrine sediment succession from the western Nanling Mountains, South China, Environmental Science and Pollution Research, 27, 20478–20489, https://doi.org/10.1007/s11356-020-08421-z, 2020.

Panagiotopoulos, K.: Late Quaternary ecosystem and climate interactions in SW Balkans inferred from Lake Prespa sediments, Universität zu Köln, Cologne, Germany, 2013.

Panagiotopoulos, K., Aufgebauer, A., Schäbitz, F., and Wagner, B.: Vegetation and climate history of the Lake Prespa region since the Lateglacial, Quaternary International, 293, 157–169, https://doi.org/10.1016/j.quaint.2012.05.048, 2013.

Panagiotopoulos, K., Böhm, A., Leng, M. J., Wagner, B., and Schäbitz, F.: Climate variability over the last 92 ka in SW Balkans from analysis of sediments from Lake Prespa, Climate of the Past, 10, 643–660, https://doi.org/10.5194/cp-10-643-2014, 2014.

Percival, L. M. E., Witt, M. L. I., Mather, T. A., Hermoso, M., Jenkyns, H. C., Hesselbo, S. P., Al-Suwaidi, A. H., Storm, M. S., Xu, W., and Ruhl, M.: Globally enhanced mercury deposition during the end-Pliensbachian extinction and Toarcian OAE: A link to the Karoo-Ferrar Large Igneous Province, Earth and Planetary Science Letters, 428, 267–280, https://doi.org/10.1016/j.epsl.2015.06.064, 2015.

Percival, L. M. E., Jenkyns, H. C., Mather, T. A., Dickson, A. J., Batenburg, S. J., Ruhl, M., Hesselbo, S. P., Barclay, R., Jarvis, I., Robinson, S. A., and Woelders, L.: Does large igneous province volcanism always perturb the mercury cycle? Comparing the records of Oceanic Anoxic Event 2 and the end-cretaceous to other Mesozoic events, American Journal of Science, 318, 799–860, https://doi.org/10.2475/08.2018.01, 2018.

Pérez-Rodríguez, M., Horák-Terra, I., Rodríguez-Lado, L., Aboal, J. R., and Martínez Cortizas, A.: Long-Term (~57 ka) controls on mercury accumulation in the souther hemisphere reconstructed using a peat record from pinheiro mire (minas gerais, Brazil), Environmental Science and Technology, 49, 1356–1364, https://doi.org/10.1021/es504826d, 2015.

Pérez-Rodríguez, M., Margalef, O., Corella, J. P., Saiz-Lopez, A., Pla-Rabes, S., Giralt, S., and Cortizas, A. M.: The role of climate: 71 ka of atmospheric mercury deposition in the southern hemisphere recorded by Rano Aroi Mire, Easter Island (Chile), Geosciences (Switzerland), 8, https://doi.org/10.3390/geosciences8100374, 2018.

Pope, R. J., Hughes, P. D., and Skourtsos, E.: Glacial history of Mt Chelmos, Peloponnesus, Greece, Geological Society Special Publication, 433, 211–236, https://doi.org/10.1144/SP433.11, 2017.

Radivojević, M. and Roberts, B. W.: Early Balkan Metallurgy: Origins, Evolution and Society, 6200–3700 BC, Springer US, 195–278 pp., https://doi.org/10.1007/s10963-021-09155-7, 2021.

Rasmussen, S. O., Bigler, M., Blockley, S. P., Blunier, T., Buchardt, S. L., Clausen, H. B., Cvijanovic, I., Dahl-Jensen, D., Johnsen, S. J., Fischer, H., Gkinis, V., Guillevic, M., Hoek, W. Z., Lowe, J. J., Pedro, J. B., Popp, T., Seierstad, I. K., Steffensen, J. P., Svensson, A. M., Vallelonga, P., Vinther, B. M., Walker, M. J. C., Wheatley, J. J., and Winstrup, M.: A stratigraphic framework for abrupt climatic changes during the Last Glacial period based on three synchronized Greenland ice-core records: Refining and extending the INTIMATE event stratigraphy, Quaternary Science Reviews, 106, 14–28, https://doi.org/10.1016/j.quascirev.2014.09.007, 2014.

Ravichandran, M.: Interactions between mercury and dissolved organic matter - A review, Chemosphere, 55, 319–331, https://doi.org/10.1016/j.chemosphere.2003.11.011, 2004.

Reimer, P. J., Austin, W. E. N., Bard, E., Bayliss, A., Blackwell, P. G., Bronk Ramsey, C., Butzin, M., Cheng, H., Edwards, R. L., Friedrich, M., Grootes, P. M., Guilderson, T. P., Hajdas, I., Heaton, T. J., Hogg, A. G., Hughen, K. A., Kromer, B., Manning, S. W., Muscheler, R., Palmer, J. G., Pearson, C., Van Der Plicht, J., Reimer, R. W., Richards, D. A., Scott, E. M., Southon, J. R., Turney, C. S. M., Wacker, L., Adolphi, F., Büntgen, U., Capano, M., Fahrni, S. M., Fogtmann-Schulz, A., Friedrich, R., Köhler, P., Kudsk, S., Miyake, F., Olsen, J., Reinig, F., Sakamoto, M., Sookdeo, A., and Talamo, S.: The IntCal20 Northern Hemisphere Radiocarbon Age Calibration Curve (0-55 cal kBP), Radiocarbon, 62, 725–757, https://doi.org/10.1017/RDC.2020.41, 2020.

Ribolini, A., Isola, I., Zanchetta, G., Bini, M., and Sulpizio, R.: Glacial features on the Galicica Mountains, Macedonia: Preliminary report, Geografia Fisica e Dinamica Quaternaria, 34, 247–255, https://doi.org/10.4461/GFDQ.2011.34.22, 2011.

Ribolini, A., Bini, M., Isola, I., Spagnolo, M., Zanchetta, G., Pellitero, R., Mechernich, S., Gromig, R., Dunai, T., Wagner, B., and Milevski, I.: An oldest dryas glacier expansion on mount pelister (former Yugoslavian Republic of Macedonia) according to 10Be cosmogenic dating, Journal of the Geological Society, 175, 100–110, https://doi.org/10.1144/jgs2017-038, 2018.

Roshan, A. and Biswas, A.: Fire-induced geochemical changes in soil: Implication for the element cycling, Science of The Total Environment, 868, 161714, https://doi.org/10.1016/j.scitotenv.2023.161714, 2023.

Rothacker, L., Dosseto, A., Francke, A., Chivas, A. R., Vigier, N., Kotarba-Morley, A. M., and Menozzi, D.: Impact of climate change and human activity on soil landscapes over the past 12,300 years, Sci Rep, 8, 247, https://doi.org/10.1038/s41598-017-18603-4, 2018.

Rousseau, D.-D., Antoine, P., and Sun, Y.: How dusty was the last glacial maximum over Europe?, Quaternary Science Reviews, 254, 106775, https://doi.org/10.1016/j.quascirev.2020.106775, 2021.

Ruszkiczay-Rüdiger, Z., Kern, Z., Temovski, M., Madarász, B., Milevski, I., and Braucher, R.: Last deglaciation in the central Balkan Peninsula: Geochronological evidence from the Jablanica Mt. (North Macedonia), Geomorphology, 351, https://doi.org/10.1016/j.geomorph.2019.106985, 2020.

Rytuba, J. J.: Mercury from mineral deposits and potential environmental impact, Environmental Geology, 43, 326–338, https://doi.org/10.1007/s00254-002-0629-5, 2003.

Sadori, L., Koutsodendris, A., Panagiotopoulos, K., Masi, A., Bertini, A., Combourieu-Nebout, N., Francke, A., Kouli, K., Kousis, I., Joannin, S., Maria Mercuri, A., Peyron, O., Torri, P., Wagner, B., Zanchetta, G., Sinopoli, G., and Donders, T. H.: Corrigendum to "Pollen-based paleoenvironmental and paleoclimatic change at Lake Ohrid (south-eastern Europe) during the past 500 ka," Biogeosciences, 13, 1423–1427, https://doi.org/10.5194/bg-13-1423-2016-corrigendum, 2016a.

Sadori, L., Koutsodendris, A., Panagiotopoulos, K., Masi, A., Bertini, A., Combourieu-Nebout, N., Francke, A., Kouli, K., Joannin, S., Mercuri, A. M., Peyron, O., Torri, P., Wagner, B., Zanchetta, G., Sinopoli, G., and Donders, T. H.: Pollen-based paleoenvironmental and paleoclimatic change at Lake Ohrid (south-eastern Europe) during the past 500 ka, Biogeosciences, 13, 1423–1437, https://doi.org/10.5194/bg-13-1423-2016, 2016b.

Sanchez Goñi, M. F. and Harrison, S. P.: Millennial-scale climate variability and vegetation changes during the Last Glacial: Concepts and terminology, Quaternary Science Reviews, 29, 2823–2827, https://doi.org/10.1016/j.quascirev.2009.11.014, 2010.

Sanei, H., Grasby, S., and Beauchamp, B.: Latest Permian mercury anomalies, Geology, 40, 63–66, 2012.

Scaillet, S., Vita-Scaillet, G., and Rotolo, S. G.: Millennial-scale phase relationships between ice-core and Mediterranean marine records: insights from high-precision 40Ar/39Ar dating of the Green Tuff of Pantelleria, Sicily Strait, Quaternary Science Reviews, 78, 141–154, https://doi.org/10.1016/j.quascirev.2013.08.008, 2013.

Schlüter, K.: Review: Evaporation of mercury from soils. An integration and synthesis of current knowledge, Environmental Geology, 39, 249–271, https://doi.org/10.1007/s002540050005, 2000.

Schneider, L., Cooke, C. A., Stansell, N. D., and Haberle, S. G.: Effects of climate variability on mercury deposition during the Older Dryas and Younger Dryas in the Venezuelan Andes, Journal of Paleolimnology, 63, 211–224, https://doi.org/10.1007/s10933-020-00111-7, 2020.

Schotsmans, E. M. J., Busacca, G., Lin, S. C., Vasić, M., Lingle, A. M., Veropoulidou, R., Mazzucato, C., Tibbetts, B., Haddow, S. D., Somel, M., Toksoy-Köksal, F., Knüsel, C. J., and Milella, M.: New insights on commemoration of the dead through mortuary and architectural use of pigments at Neolithic Çatalhöyük, Turkey, Sci Rep, 12, 4055, https://doi.org/10.1038/s41598-022-07284-3, 2022.

Schuster, P. F., Schaefer, K. M., Aiken, G. R., Antweiler, R. C., Dewild, J. F., Gryziec, J. D., Gusmeroli, A., Hugelius, G., Jafarov, E., Krabbenhoft, D. P., Liu, L., Herman-Mercer, N., Mu, C., Roth, D. A., Schaefer, T., Striegl, R. G., Wickland, K. P., and Zhang, T.: Permafrost Stores a Globally Significant Amount of Mercury, Geophysical Research Letters, 45, 1463–1471, https://doi.org/10.1002/2017GL075571, 2018.

Schütze, M., Tserendorj, G., Pérez-Rodríguez, M., Rösch, M., and Biester, H.: Prediction of Holocene mercury accumulation trends by combining palynological and geochemical records of lake sediments (Black Forest, Germany), Geosciences (Switzerland), 8, https://doi.org/10.3390/geosciences8100358, 2018.

Selin, N. E.: Global biogeochemical cycling of mercury: a review, Annual Review of Environmental Resources, 34, 43–63, 2009.

Shakesby, R. A.: Post-wildfire soil erosion in the Mediterranean: Review and future research directions, Earth-Science Reviews, 105, 71–100, https://doi.org/10.1016/j.earscirev.2011.01.001, 2011.

Shen, J., Feng, Q., Algeo, T. J., Liu, J., Zhou, C., Wei, W., Liu, J., Them, T. R., Gill, B. C., and Chen, J.: Sedimentary host phases of mercury (Hg) and implications for use of Hg as a volcanic proxy, Earth and Planetary Science Letters, 543, 116333, https://doi.org/10.1016/j.epsl.2020.116333, 2020.

Sial, A. N., Lacerda, L. D., Ferreira, V. P., Frei, R., Marquillas, R. A., Barbosa, J. A., Gaucher, C., Windmöller, C. C., and Pereira, N. S.: Mercury as a proxy for volcanic activity during extreme environmental turnover: The Cretaceous-Paleogene transition, Palaeogeography, Palaeoclimatology, Palaeoecology, 387, 153–164, https://doi.org/10.1016/j.palaeo.2013.07.019, 2013.

Simonsen, M. F., Baccolo, G., Blunier, T., Borunda, A., Delmonte, B., Frei, R., Goldstein, S., Grinsted, A., Kjær, H. A., Sowers, T., Svensson, A., Vinther, B., Vladimirova, D., Winckler, G., Winstrup, M., and Vallelonga, P.: East Greenland ice core dust record reveals timing of Greenland ice sheet advance and retreat, Nature Communications, 10, https://doi.org/10.1038/s41467-019-12546-2, 2019.

Soerensen, Anne. L., Schartup, A. T., Gustafsson, E., Gustafsson, B. G., Undeman, E., and Björn, E.: Eutrophication Increases Phytoplankton Methylmercury Concentrations in a Coastal Sea—A Baltic Sea Case Study, Environ. Sci. Technol., 50, 11787–11796, https://doi.org/10.1021/acs.est.6b02717, 2016.

Stern, G. A., Sanei, H., Roach, P., DeLaronde, J., and Outridge, P. M.: Historical Interrelated Variations of Mercury and Aquatic Organic Matter in Lake Sediment Cores from a Subarctic Lake in Yukon, Canada: Further Evidence toward the Algal-Mercury Scavenging Hypothesis, Environ. Sci. Technol., 43, 7684–7690, https://doi.org/10.1021/es902186s, 2009.

Streets, D. G., Horowitz, H. M., Lu, Z., Levin, L., Thackray, C. P., and Sunderland, E. M.: Five hundred years of anthropogenic mercury: spatial and temporal release profiles*, Environ. Res. Lett., 14, 084004, https://doi.org/10.1088/1748-9326/ab281f, 2019.

Styllas, M. N., Schimmelpfennig, I., Benedetti, L., Ghilardi, M., Aumaître, G., Bourlès, D., and Keddadouche, K.: Late-glacial and Holocene history of the northeast Mediterranean mountains - New insights from in situ-produced 36 Cl-based cosmic ray exposure dating of paleo-glacier deposits on Mount Olympus, Greece, Quaternary Science Reviews, 193, 244–265, https://doi.org/10.1016/j.quascirev.2018.06.020, 2018.

Takenaka, C., Shibata, H., Tomiyasu, T., Yasumatsu, S., and Murao, S.: Effects of forest fires on mercury accumulation in soil at the artisanal small-scale gold mining, Environ Monit Assess, 193, 699, https://doi.org/10.1007/s10661-021-09394-3, 2021.

Them, T. R., Jagoe, C. H., Caruthers, A. H., Gill, B. C., Grasby, S. E., Gröcke, D. R., Yin, R., and Owens, J. D.: Terrestrial sources as the primary delivery mechanism of mercury to the oceans across the Toarcian Oceanic Anoxic Event (Early Jurassic), Earth and Planetary Science Letters, 507, 62–72, https://doi.org/10.1016/j.epsl.2018.11.029, 2019.

Thienemann, M., Masi, A., Kusch, S., Sadori, L., John, S., Francke, A., Wagner, B., and Rethemeyer, J.: Organic geochemical and palynological evidence for Holocene natural and anthropogenic environmental change at Lake Dojran (Macedonia/Greece), The Holocene, 27, 1103–1114, https://doi.org/10.1177/0959683616683261, 2017.

Tisserand, D., Guédron, S., Viollier, E., Jézéquel, D., Rigaud, S., Campillo, S., Sarret, G., Charlet, L., and Cossa, D.: Mercury, organic matter, iron, and sulfur co-cycling in a ferruginous meromictic lake, Applied Geochemistry, 146, 105463, https://doi.org/10.1016/j.apgeochem.2022.105463, 2022.

Tzedakis, P. C., Hooghiemstra, H., and Pälike, H.: The last 1.35 million years at Tenaghi Philippon: revised chronostratigraphy and long-term vegetation trends, Quaternary Science Reviews, 25, 3416–3430, https://doi.org/10.1016/j.quascirev.2006.09.002, 2006.

Újvári, G., Kovács, J., Varga, G., Raucsik, B., and Marković, S. B.: Dust flux estimates for the Last Glacial Period in East Central Europe based on terrestrial records of loess deposits: A review, Quaternary Science Reviews, 29, 3157–3166, https://doi.org/10.1016/j.quascirev.2010.07.005, 2010.

Ulfers, A., Zeeden, C., Wagner, B., Krastel, S., Buness, H., and Wonik, T.: Borehole logging and seismic data from Lake Ohrid (North Macedonia/Albania) as a basis for age-depth modelling over the last one million years, Quaternary Science Reviews, 276, 107295, https://doi.org/10.1016/j.quascirev.2021.107295, 2022.

United Nations Environment Programme: Global Mercury Assessment, United Nations, 2018.

Vandal, G. M., Fitzgerald, W. F., Boutron, C. F., and Candelone, J. P.: Variations in mercury deposition to Antarctica over the past 34,000 years, Nature, 362, 621–623, https://doi.org/10.1038/362621a0, 1993.

Vogel, H., Wagner, B., Zanchetta, G., Sulpizio, R., and Rosén, P.: A paleoclimate record with tephrochronological age control for the last glacial-interglacial cycle from Lake Ohrid, Albania and Macedonia, Journal of Paleolimnology, 44, 295–310, https://doi.org/10.1007/s10933-009-9404-x, 2010.

Wagner, B., Lotter, A. F., Nowaczyk, N., Reed, J. M., Schwalb, A., Sulpizio, R., Valsecchi, V., Wessels, M., and Zanchetta, G.: A 40,000-year record of environmental change from ancient Lake Ohrid (Albania and Macedonia), Journal of Paleolimnology, 41, 407–430, https://doi.org/10.1007/s10933-008-9234-2, 2009.

Wagner, B., Vogel, H., Zanchetta, G., and Sulpizio, R.: Environmental change within the Balkan region during the past ca. 50 ka recorded in the sediments from lakes Prespa and Ohrid, Biogeosciences, 7, 3187–3198, https://doi.org/10.5194/bg-7-3187-2010, 2010.

Wagner, B., Aufgebauer, A., Vogel, H., Zanchetta, G., Sulpizio, R., and Damaschke, M.: Late Pleistocene and Holocene contourite drift in Lake Prespa (Albania/F.Y.R. of Macedonia/Greece), Quaternary International, 274, 112–121, https://doi.org/10.1016/j.quaint.2012.02.016, 2012.

Wagner, B., Leng, M. J., Wilke, T., Böhm, A., Panagiotopoulos, K., Vogel, H., Lacey, J. H., Zanchetta, G., and Sulpizio, R.: Distinct lake level lowstand in Lake Prespa (SE Europe) at the time of the 74 (75) ka Toba eruption, Climate of the Past, 10, 261–267, https://doi.org/10.5194/cp-10-261-2014, 2014a.

Wagner, B., Wilke, T., Krastel, S., Zanchetta, G., Sulpizio, R., Reicherter, K., Leng, M. J., Grazhdani, A., Trajanovski, S., Francke, A., Lindhorst, K., Levkov, Z., Cvetkoska, A., Reed, J. M., Zhang, X., Lacey, J. H., Wonik, T., Baumgarten, H., and Vogel, H.: The SCOPSCO drilling project recovers more than 1.2 million years of history from Lake Ohrid, Sci. Dril., 17, 19–29, https://doi.org/10.5194/sd-17-19-2014, 2014b.

Wagner, B., Vogel, H., Francke, A., Friedrich, T., Donders, T., Lacey, J. H., Leng, M. J., Regattieri, E., Sadori, L., Wilke, T., Zanchetta, G., Albrecht, C., Bertini, A., Combourieu-Nebout, N., Cvetkoska, A., Giaccio, B., Grazhdani, A., Hauffe, T., Holtvoeth, J., Joannin, S., Jovanovska, E., Just, J., Kouli, K., Kousis, I., Koutsodendris, A., Krastel, S., Lagos, M., Leicher, N., Levkov, Z., Lindhorst, K., Masi, A., Melles, M., Mercuri, A. M., Nomade, S., Nowaczyk, N., Panagiotopoulos, K., Peyron, O.,

Reed, J. M., Sagnotti, L., Sinopoli, G., Stelbrink, B., Sulpizio, R., Timmermann, A., Tofilovska, S., Torri, P., Wagner-Cremer, F., Wonik, T., and Zhang, X.: Mediterranean winter rainfall in phase with African monsoons during the past 1.36 million years, Nature, 573, 256–260, https://doi.org/10.1038/s41586-019-1529-0, 2019.

Wagner, B., Tauber, P., Francke, A., Leicher, N., Binnie, S. A., Cvetkoska, A., Jovanovska, E., Just, J., Lacey, J. H., Levkov, Z., Lindhorst, K., Kouli, K., Krastel, S., Pana-giotopoulos, K., Ulfers, A., Zaova, D., Donders, T. H., Grazhdani, A., Koutsodendris, A., Leng, M. J., Sadori, L., Scheinert, M., Vogel, H., Wonik, T., Zanchetta, G., and Wilke, T.: The geodynamic and limnological evolution of Balkan Lake Ohrid, possibly the oldest extant lake in Europe, Boreas, bor.12601, https://doi.org/10.1111/bor.12601, 2022.

Wang, F., Outridge, P. M., Feng, X., Meng, B., Heimbürger-Boavida, L. E., and Mason, R. P.: How closely do mercury trends in fish and other aquatic wildlife track those in the atmosphere? – Implications for evaluating the effectiveness of the Minamata Convention, Science of the Total Environment, 674, 58–70, https://doi.org/10.1016/j.scitotenv.2019.04.101, 2019.

Warrier, A. K., Pednekar, H., Mahesh, B. S., Mohan, R., and Gazi, S.: Sediment grain size and surface textural observations of quartz grains in late quaternary lacustrine sediments from Schirmacher Oasis, East Antarctica: Paleoenvironmental significance, Polar Science, 10, 89–100, https://doi.org/10.1016/j.polar.2015.12.005, 2016.

Watanabe, T., Naraoka, H., Nishimura, M., and Kawai, T.: Biological and environmental changes in Lake Baikal during the late Quaternary inferred from carbon, nitrogen and sulfur isotopes, Earth and Planetary Science Letters, 222, 285–299, https://doi.org/10.1016/j.epsl.2004.02.009, 2004.

Woodward, J. C., Hamlin, R. H. B., Macklin, M. G., Hughes, P. D., and Lewin, J.: Glacial activity and catchment dynamics in northwest Greece: Long-term river behaviour and the slackwater sediment record for the last glacial to interglacial transition, Geomorphology, 101, 44–67, https://doi.org/10.1016/j.geomorph.2008.05.018, 2008.

Zaferani, S. and Biester, H.: Mercury Accumulation in Marine Sediments – A Comparison of an Upwelling Area and Two Large River Mouths, Front. Mar. Sci., 8, 732720, https://doi.org/10.3389/fmars.2021.732720, 2021.

Zanchetta, G., Giaccio, B., Bini, M., and Sarti, L.: Tephrostratigraphy of Grotta del Cavallo, Southern Italy: Insights on the chronology of Middle to Upper Palaeolithic transition in the Mediterranean, Quaternary Science Reviews, 182, 65–77, https://doi.org/10.1016/j.quascirev.2017.12.014, 2018.

Zhang, Q., Huang, J., Wang, F., Mark, L., Xu, J., Armstrong, D., Li, C., Zhang, Y., and Kang, S.: Mercury distribution and deposition in glacier snow over Western China, Environmental Science and Technology, 46, 5404–5413, https://doi.org/10.1021/es300166x, 2012.